geosciences

MDPI

Article

The Effects of Facies Variability and Bioturbation Intensity on Permeability in a Mixed Siliciclastic–Carbonate Core from the Upper Strawn Group, Katz Field, Eastern Shelf of the Permian Basin, Texas, USA

Jerry L. Jensen *, Peter P. Flaig and Kelly E. Hattori

Bureau of Economic Geology, The University of Texas at Austin, Austin, TX 78758, USA; peter.flaig@beg.utexas.edu (P.P.F.); kelly.hattori@beg.utexas.edu (K.E.H.)
* Correspondence: jerry.jensen@beg.utexas.edu

Abstract: For oil and gas reservoir characterization, permeability prediction is indispensable because it helps identify potential flow pathways and lowers risk. Estimating permeability in heterogeneous media is challenging due to the limited number of measurement tools, low-resolution sampling methods, and sampling bias. To combat these issues, we employed a probe permeameter to produce a high-resolution (4 in [10 cm] spacing) permeability dataset for cores from the Strawn Formation, Katz Field, Permian Basin, Texas, USA. We structured our sampling to record permeability changes related to facies variability and fluctuating bioturbation intensity. We compared probe permeameter data to wireline logs and core-plug porosity and permeability data recorded at larger spacings. The results show that permeability is affected by facies type, bioturbation intensity, and cementation. The effects of bioturbation are non-linear; in our study, moderate bioturbation enhances permeability by improving connections between sands while intense bioturbation decreases permeability by redistributing fines. Core-plug and probe measurements gave similar permeability values, but the number of core plugs taken in the finer-grained intervals was insufficient. The probe, however, provided better resolution and gave larger net-to-gross sand ratios than core-plug-based evaluations. Using only the core-plug porosity–permeability relationship with wireline density log porosities led to permeability predictions too large by a factor of three or more compared to averaged probe permeameter values.

Keywords: tidal delta; Permian Basin; Pennsylvanian; probe permeameter; core analysis; reservoir characterization

check for updates

Citation: Jensen, J.L.; Flaig, P.P.; Hattori, K.E. The Effects of Facies Variability and Bioturbation Intensity on Permeability in a Mixed Siliciclastic–Carbonate Core from the Upper Strawn Group, Katz Field, Eastern Shelf of the Permian Basin, Texas, USA. *Geosciences* **2024**, *14*, 339. https://doi.org/10.3390/geosciences14120339

Academic Editor: Tadeusz Marek Peryt

Received: 13 September 2024
Revised: 3 December 2024
Accepted: 4 December 2024
Published: 10 December 2024

Copyright: © 2024 by the authors. Licensee MDPI, Basel, Switzerland. This article is an open access article distributed under the terms and conditions of the Creative Commons Attribution (CC BY) license (https://creativecommons.org/licenses/by/4.0/).

1. Introduction

Integrating drill core-plug and wireline well-log measurements is commonplace when analyzing reservoir quality in subsurface datasets used for conventional reservoir characterization. Routine analyses to predict reservoir presence and reservoir quality typically combine core-plug porosity and plug permeability measurements with their wireline-log proxies and employ comparisons between the analyses of these data types. This process, although integrative, may not be sufficiently detailed with respect to resolution to accurately capture transitional characteristics across key facies changes and may not accurately represent the complete evolution of rock properties through time.

Insufficient resolution in core analysis typically results from the human qualitative choices, economics, and mechanical limitations involved in the core-plug sampling method. For example, there may be bias in the choice of sampling locations and spacing along a vertical core transect because preference is given to coring well-consolidated sediments and sand-rich, carbonate-rich, and/or mud-poor intervals. Rock characteristics of cored intervals may also bias sample collection, with some intervals being fractured, poorly

indurated, or damaged and unable to be sampled in plugs. Economic considerations arise because every core plug creates costs to extract and measure. Thus, sampling programs may overlook heterogeneity and reduce sample numbers in the interests of economy. It is well established that facies heterogeneity in reservoirs affects productivity and increases risk (e.g., [1–3]).

Core-plug analysis is also an inherently destructive process that damages the core. Thus, the preferred analysis techniques for many core facilities are those that are non-destructive. A tool such as a probe permeameter (Figure 1) provides a non-destructive, relatively high-resolution technique that returns data that can be compared to core-plug-based and wireline-log-derived lower-resolution permeability data for the same well core. Specifically, probe permeameter measurements offer the opportunity to collect a higher-resolution dataset for key intervals that neither core plugs nor wireline logs may provide.

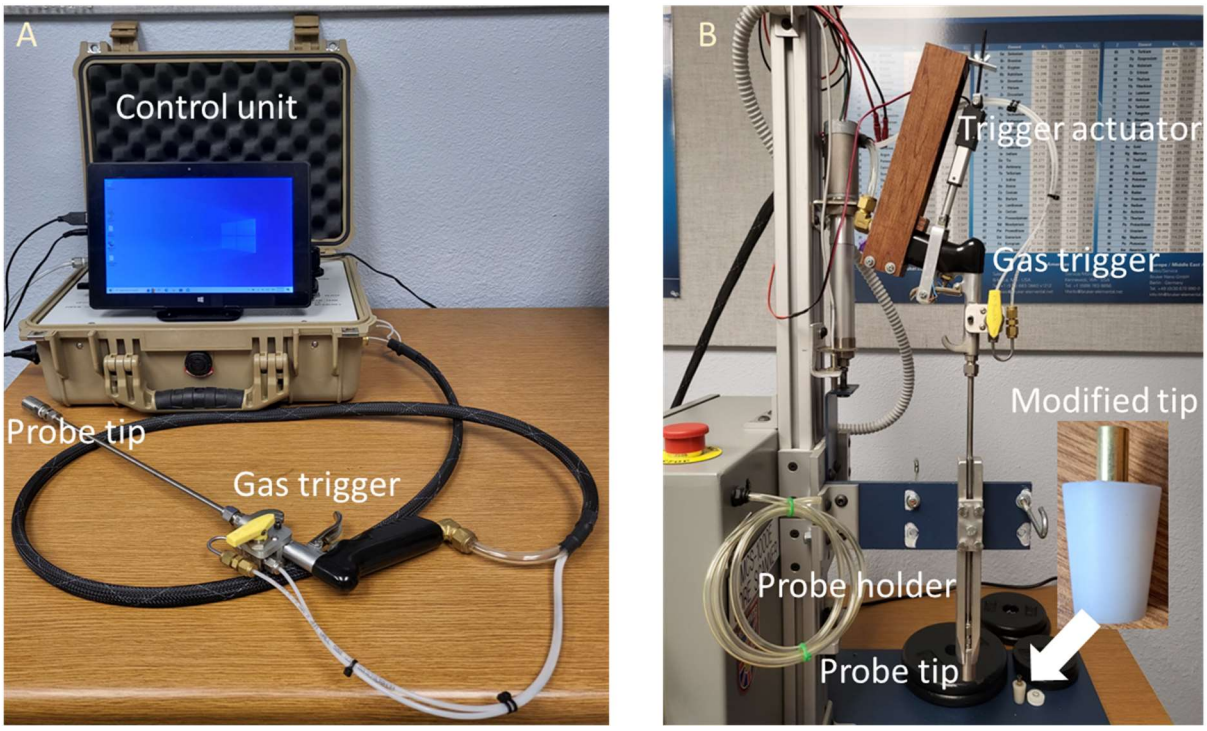

Figure 1. (**A**) CoreLabs PPP-250^{TM} probe permeameter with its main components identified. (**B**) Instrument mounted in motorized (for up–down motion and trigger actuation) fixture for measurements, with the modified tip positioned next to the probe tip.

While perhaps less familiar than core-plug or whole-core measurements, probe permeameter data have long contributed to reservoir characterization studies. Reference [4] is perhaps the first published study using probe data to examine the effects of permeability heterogeneity on waterflood recovery. Reference [5] lists 79 public-domain papers and 39 theses or academic reports covering the technical advancements and applications of probe permeameters up to 1995. Since then, nearly 100 further papers have included the use of a probe permeameter in such studies.

In general, reservoir characterization studies use the probe permeameter because it offers non-destructive measurements at a level of detail that is difficult to achieve with other methods, such as those that use core plugs or whole cores. The level of detail can be chosen to coincide with the geological stratal architecture rather than a fixed spacing, e.g., one foot or 25 cm, which is based less on geology and more on economics and mechanical considerations. Of course, probe measurements also have limitations, with the principal one being that they are shallow measurements and therefore sensitive to surface conditions, e.g., dust and residual fluids.

Although Pennsylvanian Strawn Group deposits are extensive across the Fort Worth, Midland, and Delaware Basins of Texas [6], the bulk of data are collected and owned by the oil and gas industry and are therefore proprietary. Published studies detailing Strawn facies, depositional system architectures and evolution, and rock characteristics are rare refs. [6–8]. Detailed studies of Strawn deposits are significant because, over a period of ninety years, Strawn reservoirs produced 1.15 billion barrels of oil and 4.49 trillion cubic feet of gas [9]. Strawn oil and gas plays extend across an area of 100,000 square miles, comprising 18,900 wells in 2500 named oil and gas fields across the state of Texas and into southeastern New Mexico. The Strawn oil province extends from the northern Fort Worth Basin across the Eastern Shelf to the Midland Basin and the Ozona Arch. The main gas plays occur in the northern Delaware Basin in New Mexico and the Val Verde Basin in Texas, as well as the southern part of the Fort Worth Basin.

The peak of drilling activity for the Strawn plays occurred in the 1980s, when 5300 wells were completed in Strawn strata, but the Strawn play remains very active. Recent drilling activity continues across the full extent of the play, and the most active counties have been Archer, Haskell, Jack, Jones, King, Stonewall, and Wichita. Since 2015, 840 wells have been completed in the Strawn, and those wells have produced 17.3 MMbbl of oil and 29.3 bcf of gas.

For this study, we examined two separate cores in the Pennsylvanian (Desmoinesian) Strawn Group collected from the Phillips Petroleum CB-Long C-16 well in the actively producing Katz Field in northeast Stonewall County in the state of Texas, USA (Figure 2). Cores from the CB-Long C-16 well were chosen because they are well indurated and relatively complete, include typical facies identified from the Katz field, are associated with wireline well logs, and contain a suite of core-plug data. Previously proprietary petroleum industry data from the CB-Long core donated by Kinder Morgan Inc. included routine core-plug porosity and plug permeability measurements taken at nominally one-foot spacing. Wireline-log resistivity, density–neutron, and gamma ray measurements were examined from CB-Long C-16 digital log data and compared to core porosity and permeability data. The lithofacies in each core were identified and described in detail, paying particular attention to bioturbation type and intensity, which may be linked to variability in rock properties [10]. We then selected six intervals representing the full spectrum of facies, degree of bioturbation, and contact styles observed in the core. These intervals were targeted for probe permeameter measurements, which served to substantially increase the resolution of permeability measurements available in key areas, as well as provide us with a means of comparing probe permeameter results to pre-existing data.

The effects of bioturbation on fluid flow is an area of increasing investigation but engineering reservoir models tend to characterize such horizons in simple terms. For example, refs [11,12] model bioturbated horizons as simple flow barriers. This approach may be sufficient if bioturbated intervals constitute only a small part of the reservoir or higher permeability horizons predominate. In low-permeability or tight reservoirs, however, bioturbated intervals may have a significant effect on fluid flow and hydrocarbon recovery, and more detailed modelling is necessary [13].

More geologically orientated studies, such as refs [10,13,14], evaluate permeabilities of bioturbated horizons and describe more complicated permeability behavior than modeling bioturbated intervals as simple flow barriers. Depending on the study, bioturbation can enhance or reduce permeability, and results suggest that bioturbation effects involve multiple factors including degree of bioturbation, burrow type, type of trace-making organism, and cement types and amounts. Only reference [10] state that they measured permeability using a probe permeameter; reference [14] used computer modelling, and ref. [13] do not identify the measurement method. Therefore, there remains considerable opportunity to assess bioturbation effects using both core-plug and probe permeameter methods and compare the results.

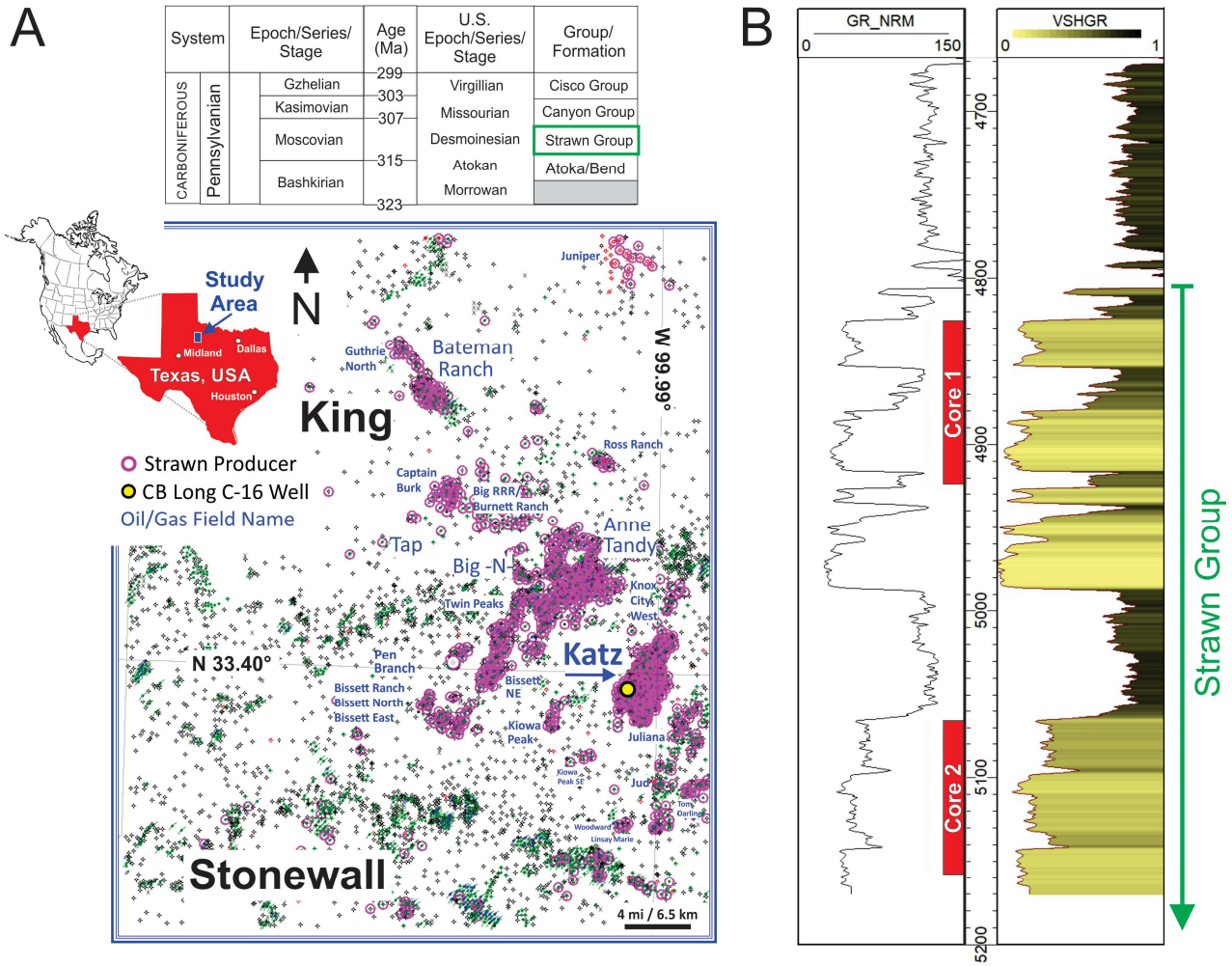

Figure 2. (**A**) Regional stratigraphic nomenclature for the Eastern Shelf of the Permian/Midland Basin and location map of local oil/gas fields including the location of the Phillips Petroleum CB-Long C-16 well in the Katz Field, Stonewall County, Texas; (**B**) normalized gamma ray log and interpolated shale volume gamma ray log from the Strawn Group interval that includes the two cores described in this manuscript. VSHGR is calculated from normalized gamma ray logs using a cutoff value of approximately 125+ API for shale. Core 1 (4825 to 4925 feet) includes the First Sand (4825–4855 feet) and the upper part of the Second Sand (4880–4990 feet), whereas Core 2 (5065 to 5157 feet) covers the upper part of the Third Sand (5065–? feet). "Sand" terminology is uniquely used by Kinder Morgan for the Katz Field.

The purposes of this study are as follows: (1) to identify facies and bioturbation trends in the CB-Long C-16 core; (2) to record probe permeameter data at relatively high resolution to test the efficacy and utility of probe-generated datasets versus traditional core-plug-based datasets; (3) to quantify the effects of facies variability and bioturbation type/intensity on permeability; (4) to evaluate and compare net-to-gross sand values using probe permeameter and core-plug data; (5) to combine data to assess the usefulness of wireline-log porosity proxies to predict permeability in non-cored wells.

Geologic Setting

The CB-Long C-16 core is one of several cores collected from the Katz Field in Stonewall County, Texas (Figure 2), and curated at the Bureau of Economic Geology, University of Texas at Austin. Discovered in 1951, the Katz Field continues to produce oil from reservoirs in the upper Strawn Group (Figure 2). The upper Strawn was deposited primarily during the Pennsylvanian (Desmoinesian) along the Eastern Shelf of the Permian Basin [6].

Deposits of the Strawn on the Eastern Shelf include interfingering, cyclic siliciclastics, and carbonates refs. [6,15]. The Katz Field is dominated by east- to northeast-sourced siliciclastic deposits with relatively minor carbonates. Deposits are interpreted as those of tidally modified deltas with crinoid-rich tidal channels, interdistributary bays, and an associated tidal shelf inboard of a carbonate ramp [16].

2. Methods

2.1. Petrophysical and Geological Data

Standard sedimentologic and ichnologic drill-core description techniques were used to identify lithofacies, interpret depositional environments, and clarify paleoenvironmental evolution of the Strawn system based on core characteristics (Table 1 and Figures 3 and 4). Bioturbation index, a measure of the degree of bioturbation that integrates sedimentology and ichnology to assess the loss of primary sedimentary fabric and increase in burrowing, was assigned based on the method of ref. [17]. Six intervals were chosen for detailed probe permeameter measurements based on a combination of facies characteristics and facies variability, as well as bioturbation intensity variability, that would be representative of the bulk of deposits found in the CB-Long C-16 core and correspond to core intervals containing available core-plug data and pertinent wireline-log characteristics (Figure 3 and Table 2). For example, select intervals were chosen based on relatively consistent facies characteristics and bioturbation intensity throughout. Alternatively, other intervals were chosen based on an overall lack of bioturbation throughout. Facies heterogeneity and variations in bioturbation intensity on the small scale are certainly present within each interval, but the goal was to choose intervals with large-scale similarities throughout.

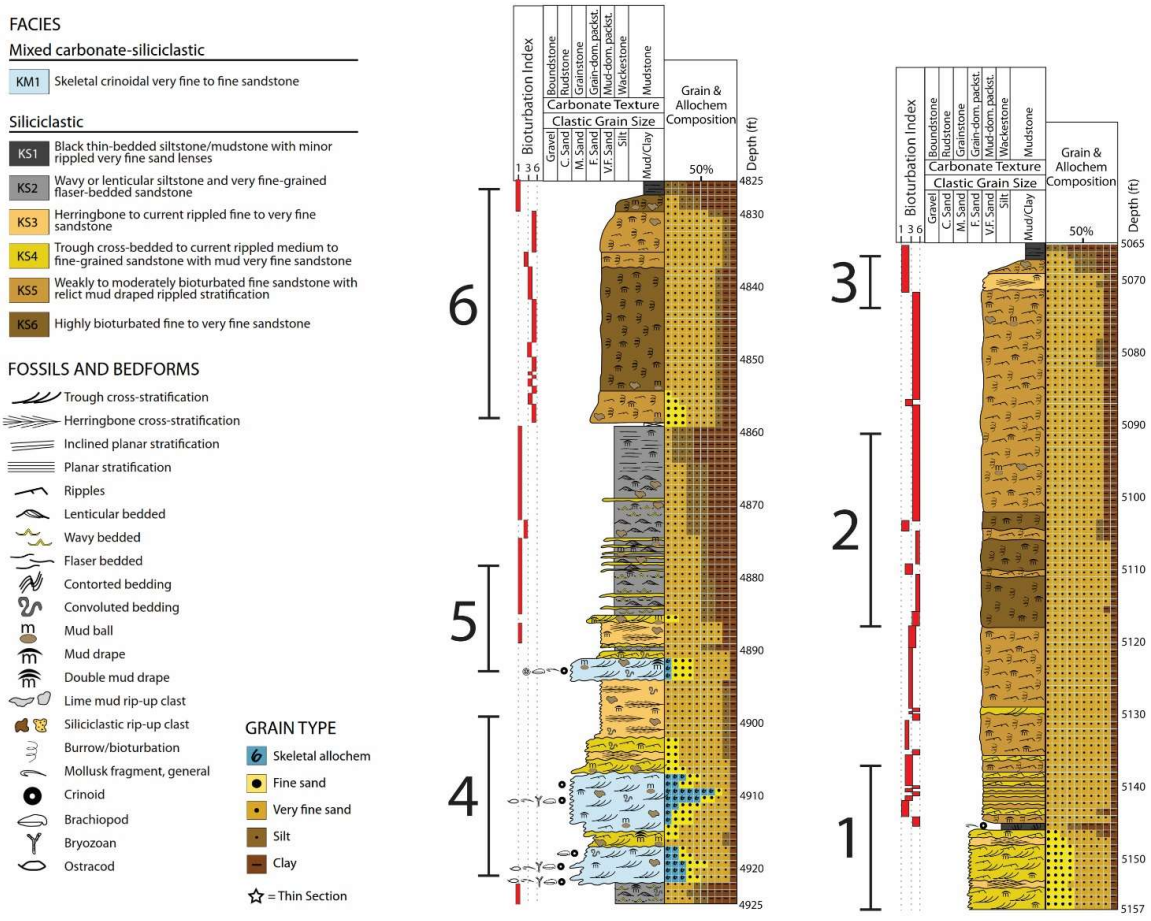

Figure 3. Stratigraphic column for the Philips C.B. Long C-16 cores including facies designations and characteristics, bioturbation index, and the six intervals chosen for detailed permeability evaluation.

Table 1. CB-Long C-16 Facies designations, descriptions, characteristics, and depositional environment interpretations.

Facies Designation	Description	Characteristics	Interpreted Depositional Environment
Mixed Carbonate/Siliciclastic			
KM1	High-angle planar-stratified to trough cross-stratified calcareous crinoid-rich fine- to medium-grained sandstone	• Medium- to silt-sized detrital quartz dominates. • Poorly sorted. • Minor lime mud < 10% • Skeletal allochems, generally concentrated in clay-rich laminae. • Common crinoids; rare brachiopods, bryozoans, and ostracods. • High-angle planar to trough cross-stratification.	Tidal channel
Siliciclastic			
KS1	Massive to thin-bedded mudstone/siltstone with rippled sand lenses, rare bioturbation	• Parallel laminations in mudstone with interbedded current-rippled sandstones. • Weakly to moderately bioturbated.	Offshore/distal prodelta
KS2	Wavy or lenticular-bedded siltstone and very fine-grained flaser-bedded sandstone	• Flaser, wavy, and lenticular bedding dominate. • Some parallel lamination. • Common siliciclastic mud clasts and rare mud balls. • Rare convolute bedding. • Single to double mud drapes on sedimentary structures. • Weakly to moderately bioturbated.	Backbarrier bay/interdistributary bay/proximal prodelta
KS3	Herringbone cross-stratified to current ripple cross-stratified fine-grained sandstone	• Dominated by herringbone cross-stratification. • Mud drapes, lime mud clasts, and convolute bedding common. • Weakly bioturbated to non-bioturbated.	Current-dominated fringes of deltas/sand-rich subtidal tidal flats, distributary mouth bars
KS4	Trough cross-stratified to current rippled cross-stratified medium- to fine-grained sandstone with mud rip-up clasts, mud balls, and mud drapes	• Largest-scale cross-stratification in siliciclastics. • Siliciclastic rip-up clasts, single and double mud drapes, and convolute bedding common. • Rarely bioturbated unless deposited in thin intervals interfingering with heavily bioturbated facies.	Channels
KS5	Weakly to moderately bioturbated fine-grained sandstone with relict mud draped ripple cross-stratification	• Current-ripple to modified current-ripple cross-stratification visible but overprinted by bioturbation. • Mud drapes, siliciclastic and lime mud clasts/balls, and convolute bedding common. • Moderately to heavily bioturbated.	Sand-rich distal tidal delta front
KS6	Highly bioturbated fine-grained sandstone	• All sedimentary structures overprinted by heavy bioturbation. • Mud drapes and siliciclastic mud clasts common. • Heavily bioturbated.	Sand-rich tidal shelf transitional to distal tidal delta front

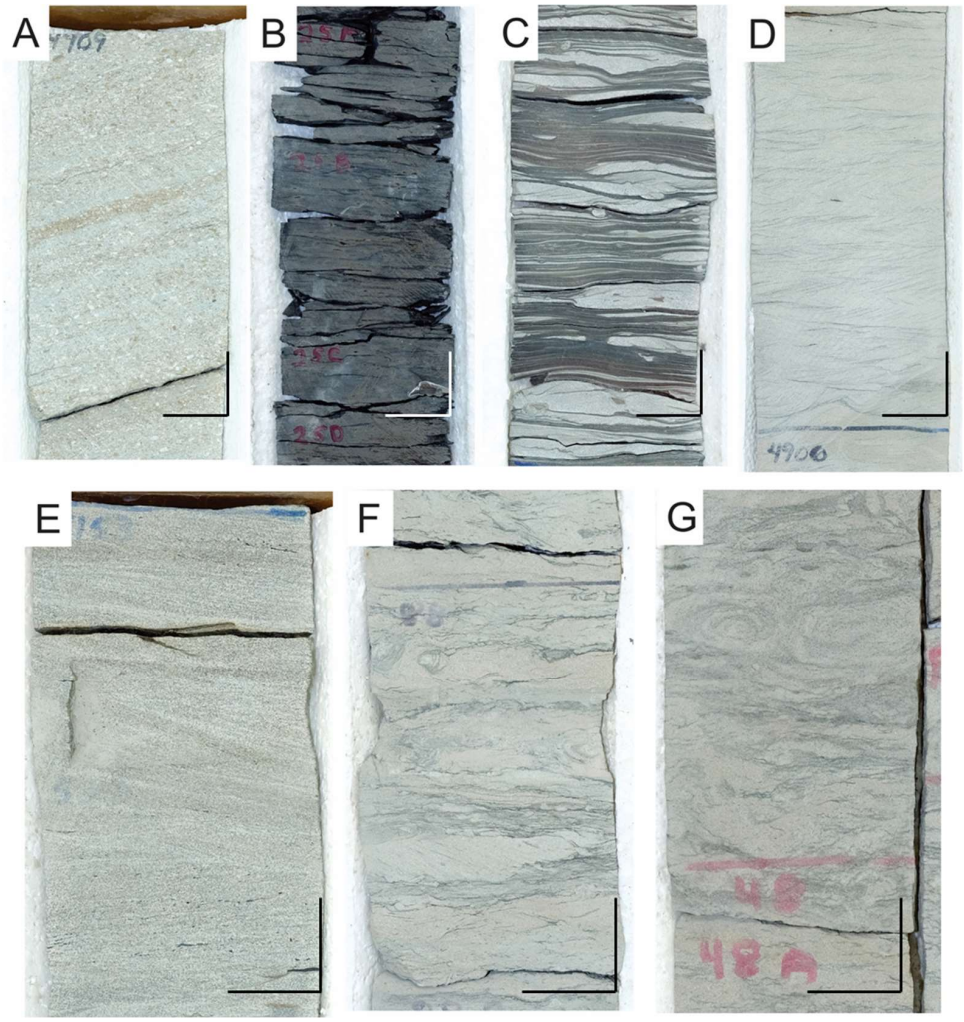

Figure 4. Examples of each facies delineated within the CB-Long C-16 core. Facies include (**A**) KM1: 4909–4910 ft, (**B**) KS1: 4825–4826 ft, (**C**) KS2: 4865–4866 ft, (D) KS3: 4899–4900 ft, (**E**) KS4: 5153–5154 ft., (**F**) KS5: 5088–5089 ft, and (**G**) KS6 4847–4848 ft: All core are standard 4 inches (10 cm) diameter core, with a cross-sectional slice that is 3 inches (7.5 cm) wide. Scale bars are one inch (2.5 cm) in both directions. See Table 1 for facies descriptions, characteristics, and paleoenvironmental interpretations.

Table 2. Core depths of intervals shown in Figure 3 and used for this study.

Interval	Base, ft	Top, ft	Total Feet
1	5157	5137	20
2	5119	5091	28
3	5073.5	5066.5	7
4	4921.5	4899	22.5
5	4893	4878	15
6	4859	4826.5	32.5

Data supplied by Kinder Morgan Inc. used in this study included routine core-plug porosity and permeability values along with wireline-log gamma ray (GR) and bulk density (RHOB) measurements. The previously collected core-plug samples were taken at approximately one-foot spacing. There were no data indicating the confining stress applied during core-plug measurements.

Grain density reported in the core-plug analyses varied from 2.63 to 2.76 g/cc with an average value of 2.67 g/cc. Wireline RHOB values from the CB-Long C-16 well were converted to porosity using the average value 2.67 g/cc. No adjustments were applied to the GR wireline values.

A commercially manufactured probe permeameter, the Core Laboratories PPP-250™ (Figure 1A) was used to measure the slabbed core permeability. The PPP-250 was modified in two ways prior to use (see [18] for more details):

1. The trigger and probe tip components were placed in a frame, and the tip placement on the core surface and trigger actuation were motorized (Figure 1B). These modifications enhance the mechanical stability of the device by keeping the tip orthogonal to the core surface and minimize tip disturbance once the tip is in place and a measurement begins.
2. The PPP-250 is supplied with a tip having an O-ring to provide sealing between the metal tip and the rock surface. A modified tip seal was used to improve tip sealing on uneven slabbed surfaces (Figure 1B). A size 1 single-hole silicone rubber stopper was placed between the tip and rock surface. The silicone stopper created a significantly better seal than the O-ring sealing element supplied with the tip.

After modification, the permeameter was found to reliably measure permeabilities from 0.02 md to 760 md. The range of measurement accuracy may be larger; however, calibrated samples were limited for testing the probe permeameter.

2.2. Probe Permeameter Measurement Strategy

Based on the guideline sampling criterion described by [19], the number of permeability measurements for each of the six selected intervals was chosen primarily based on permeability heterogeneity within each interval (Tables 2 and 3). The heterogeneity, using the coefficient of variation (C_V), was evaluated using the core-plug permeabilities:

$$C_V = \frac{1}{\sqrt{N-1}}\left[\sum_{i=1}^{i=N}\left(k_i - \overline{k}\right)^2\right]^{1/2} / \overline{k} \quad (1)$$

where k_i (i = 1, 2, …, N) are the core-plug permeabilities within an interval and $\overline{k}$ is the arithmetic average permeability. The C_V value for each interval was then used in the ref. [19] N_0 rule:

$$N_0 = \left(200 C_V / p\right)^2 \quad (2)$$

where p is the percentage desired tolerance and N_0 is the recommended number of samples. Desired tolerance is defined as follows: when N_0 samples are used to calculate $\overline{k}$, the probability that $\overline{k}$ is within p percent of the true mean is approximately 95%. See [20], p. 133–135, for more details and assumptions behind Equation (2). Typically, p = 20% is used for clastics, and p = 50% is used for carbonates [21]. A different value is used for carbonates because carbonate permeability tends to be more variable than in siliciclastic sediments. Sampling budgets, logistics, and time considerations often preclude the p = 20% choice for carbonates. For the intervals chosen, $C_V > 1$ for all but Interval 5 (Table 3), indicating these intervals are highly heterogeneous, and the tolerance needs to be relaxed to 50%.

Table 3. Intervals and their core-plug porosity and permeability characteristics for sampling using the N_0 rule. Note the different units on the sample spacing for permeability versus porosity.

				Permeability			Porosity		
Interval	**Top Depth, ft**	**Base Depth, ft**	***N* Plugs**	C_V	N_0	**Sample Spacing, in**	C_V	N_0	**Sample Spacing, ft**
6	4826.5	4859	30	1.39	31	12.7	0.27	1	28.3
5	4878	4893	8	0.72	8	21.5	0.05	0	323.5

Table 3. *Cont.*

				Permeability			Porosity		
Interval	**Top Depth, ft**	**Base Depth, ft**	***N* Plugs**	C_V	N_0	**Sample Spacing, in**	C_V	N_0	**Sample Spacing, ft**
4	4899	4921.5	22	1.59	40	6.7	0.55	5	4.6
3	5066.5	5073.5	6	1.16	22	3.9	0.40	3	2.8
2	5091	5119	28	2.04	66	5.1	0.25	1	27.3
1	5137	5157	20	1.16	21	11.2	0.57	5	3.9

3. Results

3.1. Facies Descriptions and Interpretations

Six siliciclastic facies and one carbonate facies were identified in the core based on discrete differences in mineralogical composition, bedforms, bioturbation, and grain types, sizes, and sorting. Table 1 contains facies designations, a brief summary of facies characteristics, and an interpretation of depositional environments represented in core based on rock characteristics, bioturbation, and stacking. Figure 3 is a stratigraphic column derived from the two different CB-Long C-16 cored intervals that shows the facies classification, and characteristics including rock type, grain size, flora, fauna, inclusions, and bioturbation index.

The only mixed carbonate/siliciclastic facies, KM1, occurs in three 3–7 ft (1 to 2 m) thick high angle planar cross-stratified beds that have been interpreted as tidal channels (Figure 4A). At the 4-inch (10 cm) resolution selected for probe permeameter analysis, 34 measurements were collected; 14 core-plug permeability measurements were available for comparison. Of the siliciclastic facies, KS1 (Figure 4B) and KS2 (Figure 4C) are largely dominated by siliciclastic mud and silt attributed to low-energy prodelta, offshore, and backbarrier bay settings. Four (4) and twenty (20) probe permeameter measurements were recorded for these two facies, respectively; in contrast, only two core plugs were analyzed from KS2, and none were analyzed for KS1. This discrepancy reflects the difficulty of sampling poorly consolidated splintery and fissile rocks such as those encountered in KS1 and KS2, and highlights an inherent bias to plug sampling that is not present in the probe permeameter methodology.

Facies KS3 (Figure 4D), KS4 (Figure 4E), KS5 (Figure 4F), and KS6 (Figure 4G) are dominated by fine- to very fine-grained quartz-rich sandstone and comprise the majority of the core; the facies differ from one another on the basis of bedforms and degree of bioturbation. All have been interpreted to reflect a tidal delta to tidal shelf marine setting. Facies KS6 is heavily bioturbated and reflects a transitional setting from the distal edge of a delta to a sand-rich tidal shelf; the lower amount of bioturbation in KS5 indicates a delta front setting with more abundant freshwater influx. KS4 and KS3 are less bioturbated and instead contain well-preserved herringbone, current ripple, and trough cross-stratification attributable to more proximal deltaic settings with more abundant freshwater input and less bioturbation. Thin section analysis of the facies permits closer investigation of how aspects of bedding, bioturbation, grain size, and composition interplay and impact porosity and permeability (Figure 5). Together, the facies provide an opportunity to investigate the role of bioturbation and bedding styles on permeability, allowing us to fine-tune our understanding of characteristics that may impact reservoir flow pathways and production.

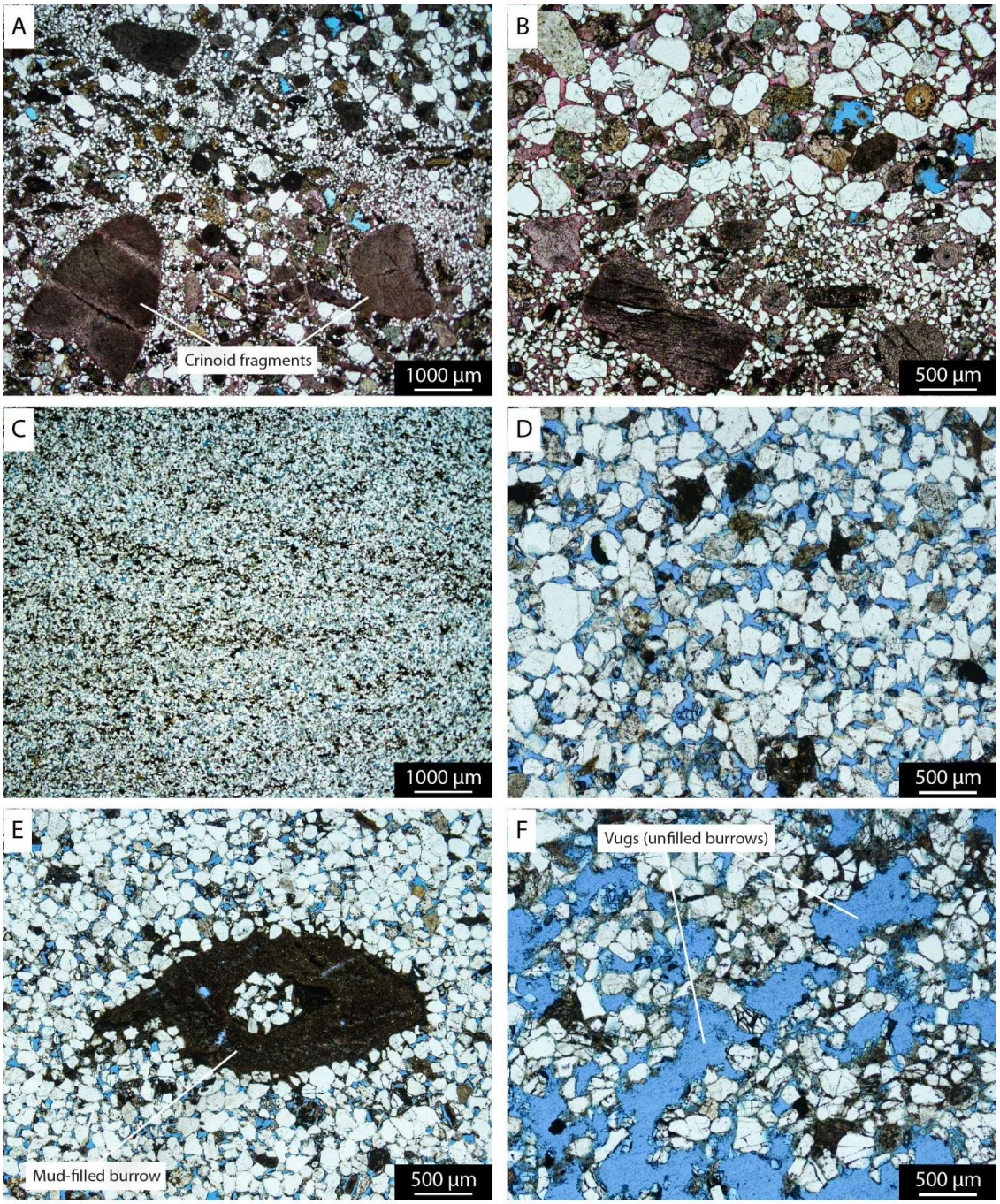

Figure 5. Thin section photomicrographs of facies) of the Katz Field. All photos captured in plane polarized light. (**A**,**B**) Facies KM1, high-angle planar-stratified calcareous crinoid-rich sandstone. Note poor sorting: large crinoid fragments are mixed with fine-grained quartz-rich sandstone and silt. Calcite cement between grains is stained in red. (**C**,**D**) Facies KS3, herringbone cross-stratified to current ripple cross-stratified fine-grained sandstone. (**C**) shows herringbone bedding; (**D**) highlights high interparticle porosity and permeability. (**E**) Facies KS5, weakly to moderately bioturbated fine-grained sandstone with relict mud draped current ripple to modified current ripple cross-stratification. Mud-filled burrow is prominent in the center of the image. (**F**) Facies KS6, highly bioturbated fine-grained sandstone. Fine-grained quartz sand exhibits significant disturbance with large vugs left behind in burrow voids. Images (**E**,**F**) highlight the potential of burrows to either hinder or enhance flow (permeability).

3.2. Evaluation of Permeability Heterogeneity and Sampling

For this study, a uniform sample spacing of four inches for probe permeameter measurements within six selected intervals (Table 3) was chosen to provide a tolerance of p = 50% or smaller. Using this criterion and comparing to the location of core plugs, core-plug sampling at one-foot intervals may have been sufficient for Intervals 1, 5, and 6 but insufficient for Intervals 2, 3, and 4. If p = 20%, the sample spacing would range from ½ inch (Interval 3) to 3½ inches (Interval 5), which would make the data collection process unreasonably time-consuming and essentially unmanageable.

The N_0 guideline can be applied to any petrophysical variable, including core-plug porosity (Table 3). The sample spacing for porosity measurements is much larger because porosity is less variable than permeability (e.g., [22], p. 44). For this core, permeability is between 2 and 13 times more variable than porosity.

Between two and four measurements at each sample location (depth) were made, with the tip of the instrument lifted and moved laterally by ½ inch (1.2 cm) or more between measurements. This choice was made for two reasons: (1) as a quality control measure to check measurement repeatability, particularly in areas with uneven surfaces; and (2) to assess cm-scale variability in the most heterolithic intervals. Approximately 83% of the adjacent values were found to be within a factor of two (Figure 6), suggesting that the probe measurements are consistently repeatable. At several depth locations, however, there are differences between Trial 1 and Trial 2 values that exceed factors of 5 and may appear anomalous. Other studies also show similar differences occasionally arise for nearby probe measurements in heterogeneous sediments. For example, reference [23] their Figure 5 report differences of factors of five or more for probe measurements taken on the end faces of a single one-inch (25 mm) core plug in cross-bedded estuarine channel dunes. Reference [19] their Figure 8b show variabilities of factors of 8 to 10 over distances of less than four inches (10 cm) for cross-stratified and heterolithic intervals. Reference [24] their Figure 4 show probe values changing by factors of 10 or 20 over four-inch (10 cm) distances.

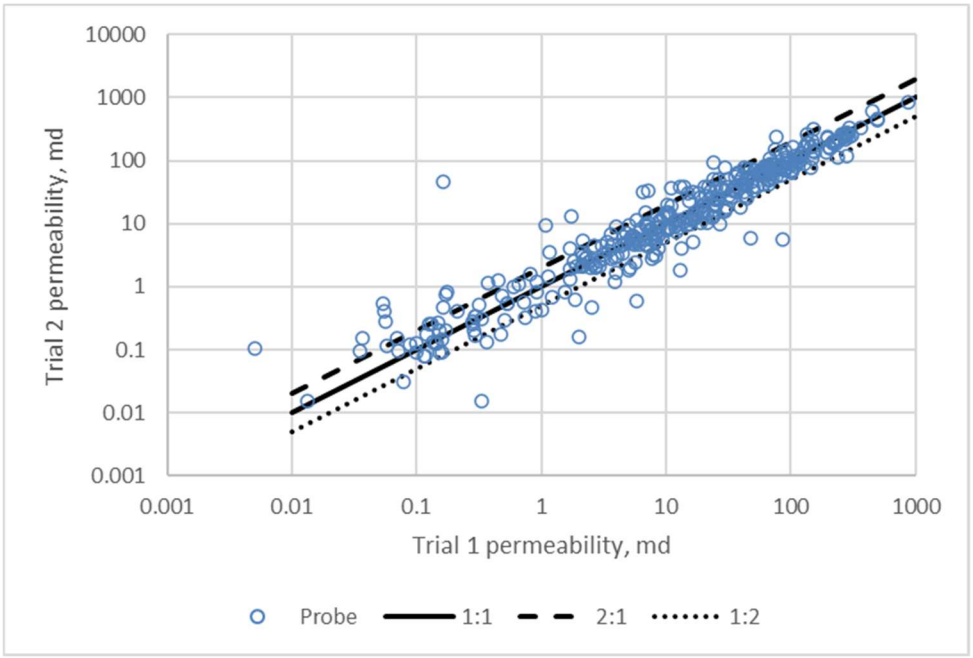

Figure 6. Comparison between the first and second measurements made with the probe permeameter at each depth. Of 359 depths measured, 62 measurement pairs differed by more than a factor of two.

In general, the levels of local variability remain similar throughout the range of permeabilities. There is, however, a subtle reduction in variability as permeability increases

above approximately 50 md, which corresponds to permeabilities coming from the coarser grained and less bioturbated facies KS3, KS4, and KS5.

3.3. Core-Plug Versus Probe Permeability

Because the original core plugs were not physically available for this study, we could not undertake a one-for-one comparison of the probe versus plug permeability values (as performed by, for example, ref. [23]). Instead, we compared plug permeability and probe permeability measurements taken from similar core depths (Figure 7). Comparisons of plug-based and probe-based average permeability values for each of the six intervals were also made (Figure 8). Because two or more probe measurements were made at each depth, we used the median value of those measurements. Our results show that:

1. Probe permeameter and plug permeabilities mostly correlate strongly, with probe values showing more variability than plug values because of the greater number of measurements at a higher resolution (Figure 7). The greatest discrepancy between probe and plug permeabilities is in Interval 2, which exhibits systematic differences between probe and plug permeabilities with the probe averaging approximately 44% higher permeabilities than plug permeabilities. Much of this interval is KS5 facies, having numerous mud-draped ripples. This difference is likely due to the differences in sample volume for the probe permeameter and core plugs. An example of this is shown in Figure 4F, where close inspection shows where a core plug was taken, with 1.02 md measured. The left side of the plugged area is darker due to the mud and shows low permeability, while the right side is lighter in color and has less mud. Nearby probe measurements have larger permeabilities, 7.7 and 5.2 md, than the core plug. The larger-volume core-plug measurement likely reflects the effects of the smallest permeability component (mud) on fluid flow, whereas the probe measurement is responding to the mud-free components. A similar effect has been observed by (ref. [25], their Figure 7) for heterolithic rocks having mud fractions in excess of approximately 20%.
2. In general, probe averages are more than one-half but less than or equal to plug average values (Figure 8). Note that, for Interval 5, probe data were acquired for core depths 4882 to 4891 feet for which no plugs were taken because of the fissile nature of the core. The comparison of averages for this interval only covered those depths for which both plug and probe measurements were made. As noted earlier, we did not have confining stress values for the core-plug permeability measurements but they will be larger than the sample stresses applied during probe measurements. If stress differences were important, the plug permeabilities would be less than the probe values but that is not the case here. Probe averages with values less than plug averages are consistent with other studies of this type (e.g., refs. [24,26,27]). Reasons for this result may include the effects of surface dust reducing the probe values, although we found no evidence for this here, and/or core-plug bias that selectively sampled higher-permeability material.

We evaluated the net sand to gross sand (NTG) ratios in five intervals having both probe and plug permeability values to assess the value of the probe's greater detail for a common petrophysical calculation (Table 4). Here, we define NTG as the ratio of net reservoir thickness to gross thickness, where net sand thickness is the sum of intervals having a permeability at or above a threshold value. Note that this definition excludes consideration of fluid types and amounts in the formation. The calculation here assumed that the net pay threshold is 1 md, a typical value used for reservoir evaluation, and a reservoir having 1 cP fluid viscosity [28]. Intervals 4 and 5 were combined for two reasons: (1) Intervals 4 and 5 have similar siliciclastic facies; (2) the carbonate facies of Interval 4 do not contribute any net pay because their permeabilities are less than 1 md.

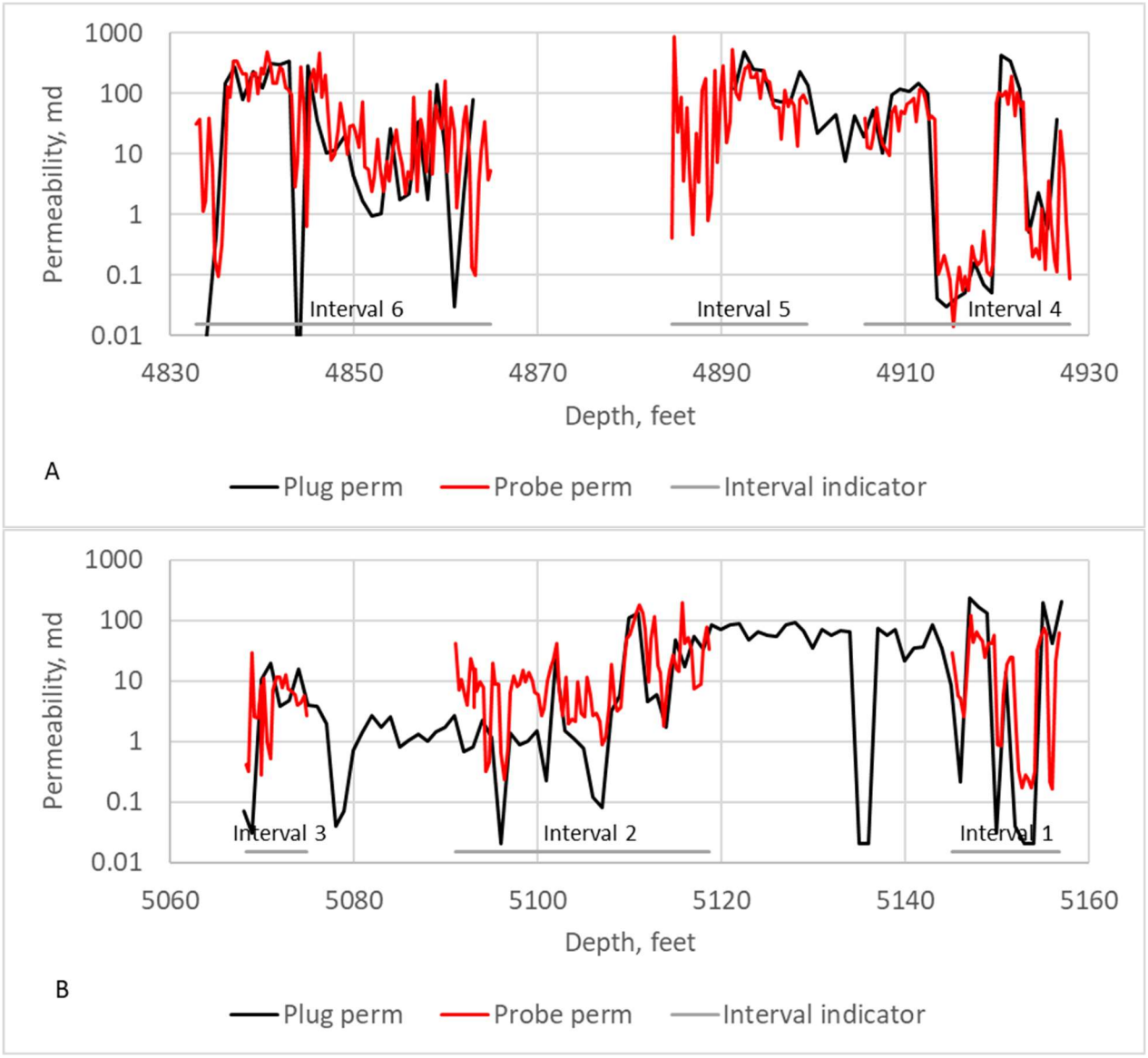

Figure 7. Core-plug and median probe permeabilities for (**A**) Intervals 4–6 and (**B**) Intervals 1–3. Depths listed on x axis are core depths. Interval indicator line shows the location of each of the intervals.

Table 4. Comparison of net sand: gross sand (NTG) ratios using probe and plug permeabilities.

Interval	From Depth, ft	To Depth, ft	NTG Plug	NTG Probe	Ratio, Percent
6	4834	4863	0.83	0.94	113
4 and 5	4891	4926	0.75	0.64	86
3	5068	5074.9	0.78	0.84	108
2	5091.5	5118.75	0.71	0.93	132
1	5137	5154.5	0.74	0.73	100

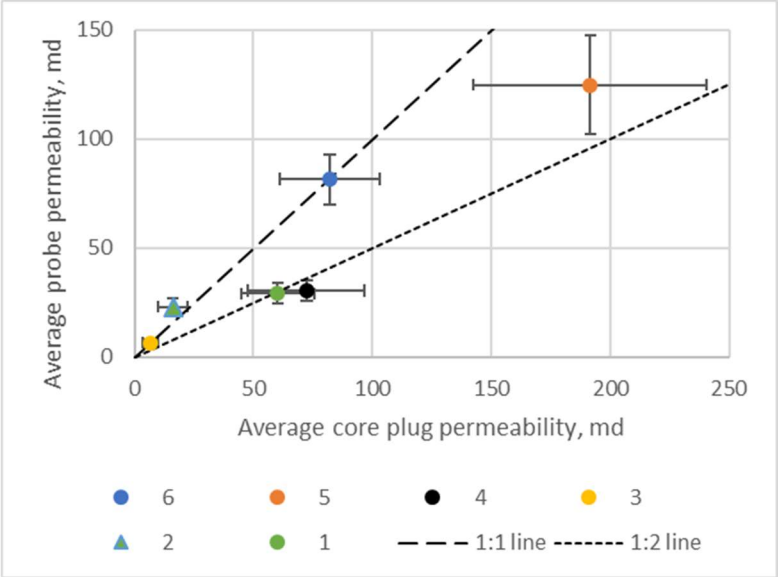

Figure 8. Comparison of plug and probe average permeabilities for each of the six intervals (labelled 1 through 6). Error bars indicate one standard error (i.e., approximately 68% probability). Standard error is defined as the estimated standard deviation of the arithmetic average.

In almost all cases, the probe-based NTG values are equal to or larger than the plug NTG values. The one exception where the probe NTG is less than the plug NTG (Table 4, line 3) is caused by the probe permeameter readings in the 4922–4925 ft interval, which have an average substantially lower than the core-plug value (0.5 md vs. 41 md). The probe exhibits considerable variability (C_V = 1.4) over this small interval of facies KS2 and the plug samples were collected selectively from the less muddy, larger permeability areas of core (Figure 4C).

3.4. Permeability–Facies Effects

Tables 5 and 6 list statistics for facies proportions and permeabilities. Blanks in the tables indicate areas with too few samples for analysis, or no samples on which to base a calculation. Most of the statistics are commonly used and familiar, except perhaps for standard error. Standard error is the standard deviation of the arithmetic average. Standard error is useful when comparing two arithmetic averages such as probe and core-plug average permeabilities because it accounts for both sample numbers and variability.

Table 5. Probe permeability statistics and approximate proportions for Strawn facies listed in Table 1. Color coding is consistent with Figure 3.

Facies	KM1	KS1	KS2	KS3	KS4	KS5	KS6
Proportion	0.08	0.03	0.13	0.08	0.14	0.36	0.08
Sample median, md	0.2	1.5	19.3	12.2	44.7	10.4	12.0
Arithmetic average, md	19.0	8.1	61.7	52.8	79.9	60.8	38.1
Standard error, md	5.8	7.0	17.0	14.8	16.2	10.0	6.7
Coef of variation C_V	1.9	1.7	1.2	1.4	1.6	1.6	1.8
Number of msmts	38	4	20	24	66	96	102

Table 6. Core-plug permeability statistics for Strawn facies listed in Table 1. Color coding is consistent with Figure 3.

Facies	KM1	KS1	KS2	KS3	KS4	KS5	KS6
Sample median, md	0.4	-	59	59	97	4.8	5.1
Arithmetic average, md	60.9	-	59	59	117	45.1	39.8
Standard error, md	33.5	-	-	-	25.7	7.7	15.7
Coef of variation C_V	2.1	-	-	-	1.0	1.4	2.2
Number of msmts	14	0	2	2	22	69	32

Facies proportions of Table 5 are based on one-foot spaced evaluations. This technique resulted in the omission of some measurements in relatively thin beds of KS4 interbedded with thicker intervals of KS2 in the interval 4859 to 4885 feet. Thus, the resultant proportion of facies KS4 is slightly too small, and the proportion of KS2 is commensurately too large. Sample numbers varied considerably among the facies. KS1 and KS2 were undersampled by the probe relative to other facies because the key intervals selected for measurement did not contain many occurrences of KS1 and KS2. KS1 and KS2 were also undersampled due to mechanical limitations on collecting plugs; consolidated samples are needed for a plug to be drilled, and some of the KS1 and KS2 intervals are not well consolidated. KS3 was also poorly sampled with respect to core plugs. KS5 and KS6, on the other hand, were well sampled by both core-plug and probe permeameter measurements, and the sample statistics agreed closely.

Heterogeneity, as defined here, is not "visual" heterogeneity as one might view overall facies heterogeneity in a core (e.g., Figure 4); instead, it is the calculated value C_V based on permeabilities (Equation (1)). Heterogeneity (C_V) levels are similar between probe and plug measurements except for KS4, where the plugs show much less permeability variability than the probe values. The KS4 core plugs may have also avoided including the muddier elements within this facies. Of all facies, KM1 and KS6 are the most heterogeneous. KS1 may be heterogeneous, but with only four measurements, C_V = 1.7 versus C_V = 1.9 may not reflect a statistically significant difference in C_V.

Comparing the above observations with Figure 4 reveals some differences. The heterogeneity assessments based on the permeability C_V do not always accord with visual assessments of heterogeneity for three possible reasons. Firstly, C_V is a relative measure of permeability variation. For example, KS1 has a small average permeability, so that a small permeability variability, as measured by the standard deviation, still gives a large C_V. Secondly, visual heterogeneity does not necessarily equate to permeability heterogeneity. The shape and extent of heterogeneities can affect permeability, which is difficult to incorporate into visual assessments. For example, consider a hypothetical layered system with horizontal fluid flow. A horizontal layered case (i.e., flow parallel to layers) of 20% muds and 80% sandstone versus a vertical layered case (i.e., flow across the layers) will have the same visual impact but quite different effects on fluid flow (e.g., refs. [20,25]). Finally, permeability can respond to variations invisible to the naked eye, such as subtle grain size changes or differences in cementation amounts and distribution.

With two exceptions, the sample medians are less than the averages for both probe and plug data (Tables 5 and 6). This suggests that the permeability probability distributions are skewed for most facies. That is, there are relatively few large permeabilities and many smaller values of permeability for most facies. The average may be less representative than the sample median for permeability in these cases (refs. [29] Chap. 3, [20] p. 118).

Using box and whisker plots, Figure 9 shows probe permeability statistics across facies. The upper and lower ends of each box represent the upper and lower sample quartiles, respectively, and the distance between the top and bottom of the box is the interquartile range (IQR). The line within each box is the sample median value. The upper

"whisker" extends to the sum of the upper quartile plus 1½ x IQR or the maximum datum, whichever is smaller. The lower whisker extends to the lower quartile minus 1½ x IQR or the minimum datum, whichever is larger. See ref. [29] p. 59–60 for more details. Comparing sample medians (Figure 9 and Table 5), Facies KM1, the carbonate facies, has the lowest permeability. Of the siliciclastic facies, Facies KS1 has the lowest permeability, and Facies KS4 has the highest permeability. Because of the logarithmic scaling of Figure 9A, small differences in graphed position may represent large differences in permeability. Therefore, a linear scaling is also shown in Figure 9B.

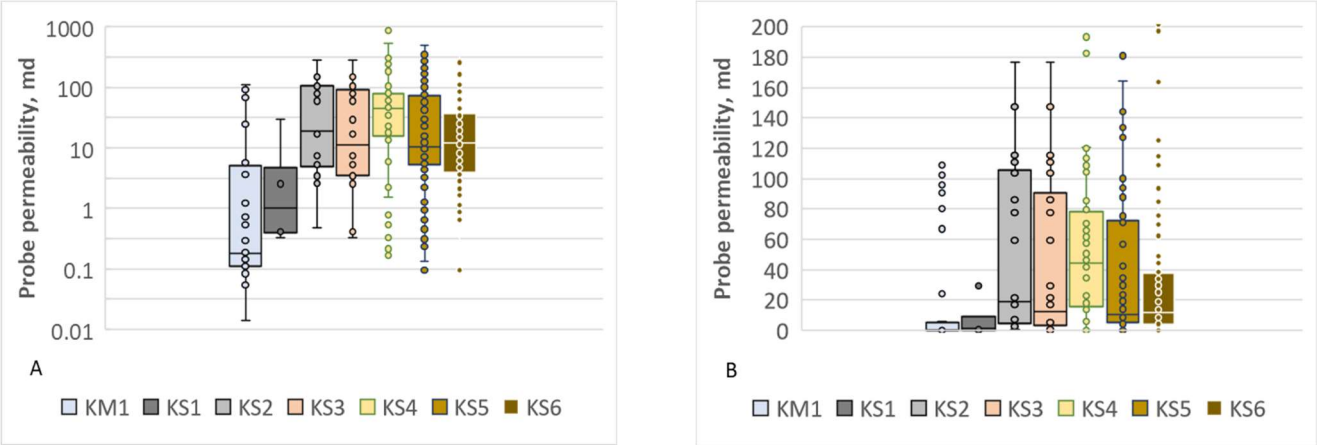

Figure 9. Box and whisker plots showing permeability statistics for each facies on (**A**) logarithmic and (**B**) linear scales. Figure 9B omits some larger outlier values. Colors are consistent with facies in Figure 3.

3.5. Permeability–Wireline-Log Correlations

As is common with siliciclastic sediments, core-plug porosity has a moderately strong linear correlation with the logarithm of core-plug permeability (Figure 10). The strong correlation of porosity to permeability at the core-plug scale may suggest that the wireline-log density porosity measurement could be a useful permeability estimator. Such an approach is attractive because porosity is easier to measure than permeability. It has been used, for example, by refs. [30,31]. However, given the degree of small-scale (cm and dm) heterogeneity of Strawn sediments in the CB-Long C-16 core, wireline-log porosity tools may lack the resolution to be an effective permeability estimator using the core-plug relationship shown in Figure 10.

To evaluate the correlation of wireline-log density porosity with probe permeability, we first calculated a thickness-weighted arithmetic average of the probe permeameter values over a one-foot window. This gave a resolution of the probe measurements that is compatible with the wireline-log density tool. Wireline-log density porosity appears to correlate moderately well with the logarithm of averaged probe permeability (Figure 11). Based on the R^2 value, however, the strength of relationship varies from interval to interval (Table 7). Intervals 2 through 4 appear moderate to strong, while Intervals 1, 5, and 6 are relatively weak. Intervals 1 and 6 have a small porosity and permeability variation compared to Intervals 2 through 4, hence R^2 may be smaller in Intervals 1 and 6 [20] p. 172, even if the underlying relationship between porosity and permeability is unchanged. Interval 5 has a large density porosity variation, but the probe permeability shows less variability. Interval 5 contains mostly silts with thin occurrences of fine sand, and is highly heterogeneous at the cm to dm scale. Interval 5 is composed of lenticular to wavy-bedded siltstones and fine-grained sandstones (except for the bottom 4 feet of fine- to medium-grained sandstone), which makes the one-foot probe permeability averaging unrepresentative of either the silt or fine- to medium-grained sand permeabilities. Similarly, the wireline porosity response poorly captures the permeability variations in the upper part of this interval.

Using unaveraged, high-density probe values, a correlation becomes evident between the wireline porosity and the permeability minima (R^2 = 0.65) (Figure 12). Without the detailed permeability variations captured by the probe measurements, understanding the limitations of the wireline porosity–permeability relationship would not be possible.

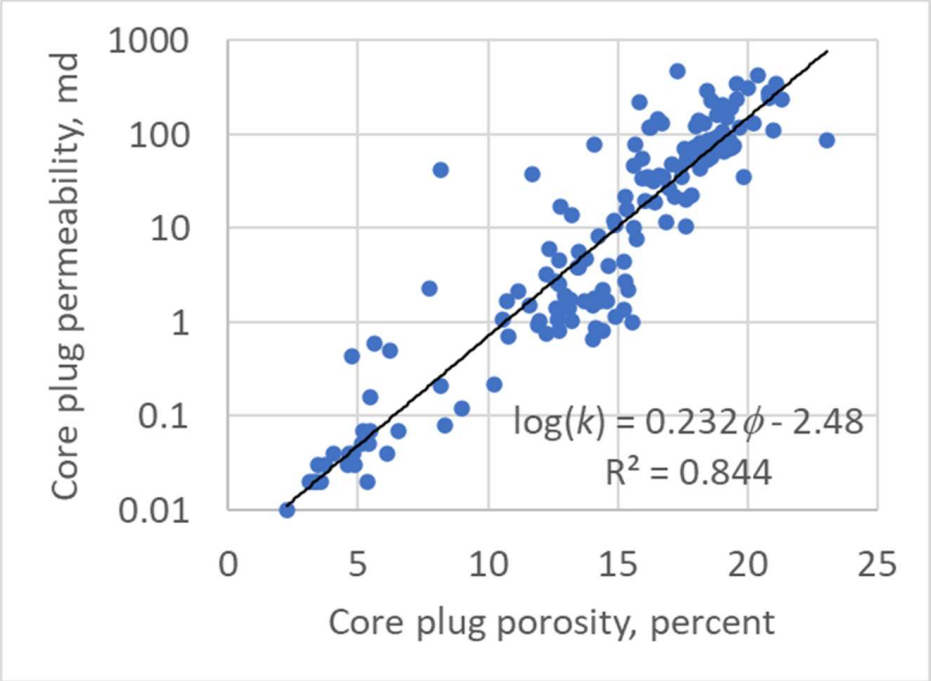

Figure 10. Core-plug porosity (ϕ) vs. permeability ($\log_{10}$ (k)) relationship with linear model (black line) fit using least squares linear regression. R^2 is the coefficient of determination.

Table 7. Wireline density vs. logarithm of one-foot averaged probe permeability relationship strength using a linear model.

Interval	Coef. of Determination, R^2
6	0.05
5	0.24
4	0.84
3	0.57
2	0.45
1	0.346

Interval 5 data also suggest that the wireline density log may not be as effective a permeability predictor as the core-plug porosity–permeability relationship (Figure 10) indicates. More generally, a comparison of the two approaches (Figure 13) shows that the core-plug porosity–permeability model poorly captures the porosity–permeability relationship at the one-foot scale. For example, the wireline porosity log combined with the core-plug porosity–permeability relationship overpredicts facies KS3, KS4, and KS5 permeabilities by at least a factor of three for porosities greater than 15%. This permeability overprediction is much larger than could be explained by the probe underpredicting the core-plug permeabilities seen for some intervals in Figure 8.

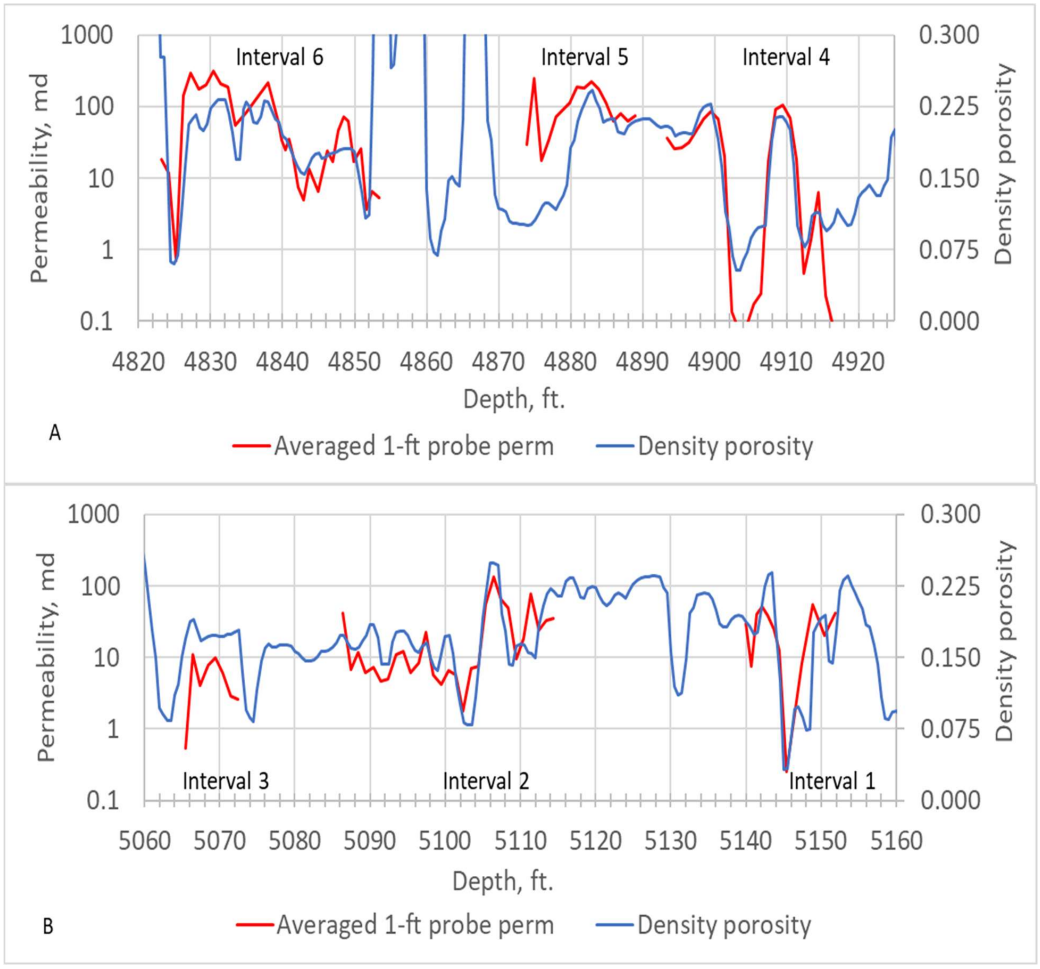

Figure 11. Density porosity versus probe permeability for (**A**) Intervals 4–6 and (**B**) Intervals 1–3. Depths are wireline-log density depths. The high-porosity interval (4852–4870 ft.) is a borehole enlargement where the logging tool's pad had poor contact with the formation.

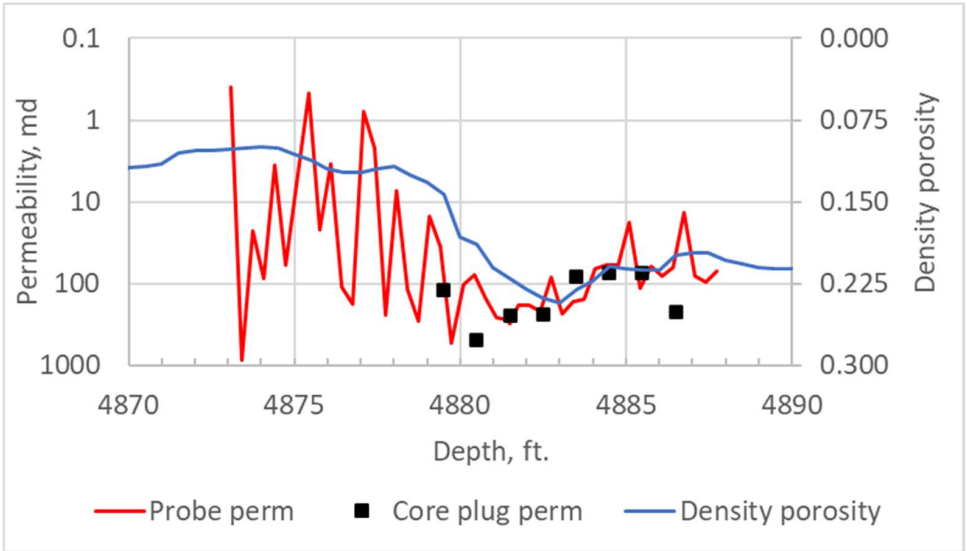

Figure 12. Interval 5 wireline density log porosity correlation with unaveraged probe permeability and core-plug values. Due to the fissile and poorly preserved nature of the core over the interval 4857 to 4880 feet, core-plug sampling was not performed in most of that interval. Depths listed are wireline depths.

Figure 13 also suggests that facies KS3, KS4, and KS5 have similar porosity–permeability relationships. The combination has a coefficient of determination $R^2 = 0.70$. These three facies comprise more than 50% of the Strawn formation in this well and more than 75% of the formation flow capacity (Table 5). Therefore, a wireline density permeability predictor may be useful for these facies but the predictor is not based on the core-plug porosity–permeability relationship (Figure 10). Facies KS6 appears to have only a weak density porosity–permeability relationship. Facies KS1 and KS2 have only minor occurrences, so the porosity–permeability relationship cannot be established. A similar situation exists for Facies KM1, where more than two-thirds of the points have permeabilities below 2 md.

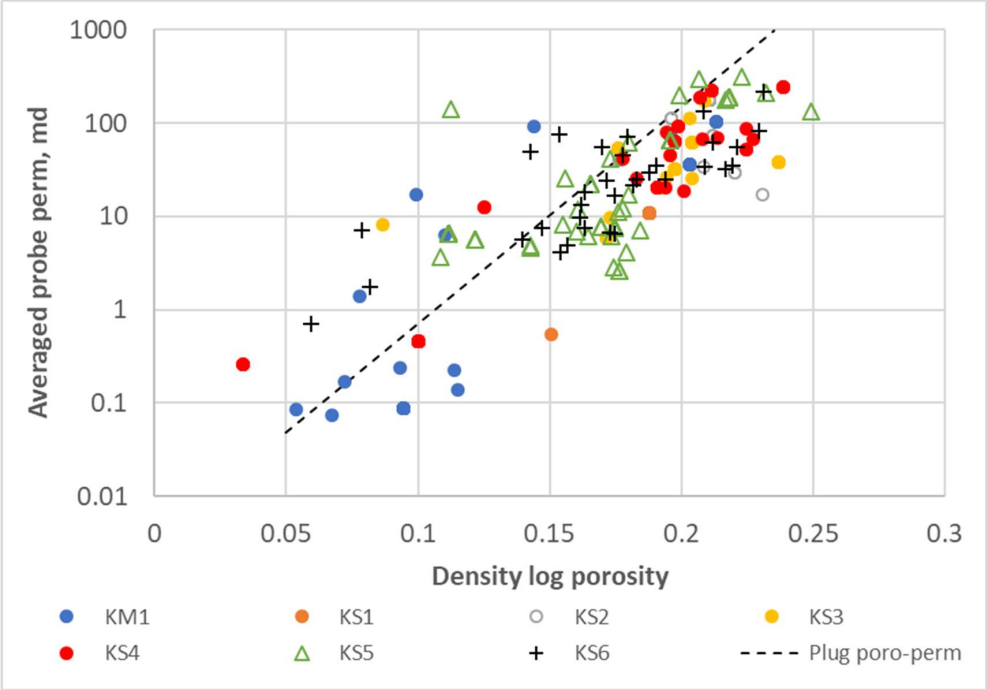

Figure 13. Density log porosity versus logarithm of one-foot averaged permeability categorized according to facies. The dashed line is the linear model shown in Figure 10.

3.6. Permeability–Bioturbation Effects

A literature review of the effects of bioturbation on permeability revealed conflicting results. For example, several studies report that even moderate bioturbation can increase permeability (e.g., refs. [32] and therein; ref. [33]). Alternatively, reference [10] suggest that there can be either increases or decreases in permeability with bioturbation, depending on whether the tracemakers are sediment cleaners, sediment packers, sediment mixers, or exhibit a combination of behaviors. We examine the effects of bioturbation on permeability using the bioturbation index (Bi) of ref. [17] to compare trends in bioturbation intensity and probe permeameter permeability measurements.

Foot-by-foot values of Bi and grain size (on a scale of 1 = clay to 5 = fine sand) were recorded over the entire CB-Long C-16 core (Figure 3). Arithmetic average probe and core-plug permeability values were calculated for sediments within intervals of interest (Figure 14). Some intervals had Bi values averaged at 1.5, reflecting a mixture of Bi = 1 and Bi = 2 sediments at a sub-foot scale, with varying degrees of bioturbation within the measurement interval. All intervals with Bi = 1, 1.5, or 2 were ultimately combined to a value of Bi = 1.5 for two reasons. First, because of the small numbers of samples; only 12 locations had Bi = 1, 16 locations had Bi = 2, and 29 locations had Bi = 1.5. Second, because the Bi = 1.5 locations represented both Bi = 1 and Bi = 2; distinguishing between Bi = 1, 1.5, and 2 would not be meaningful.

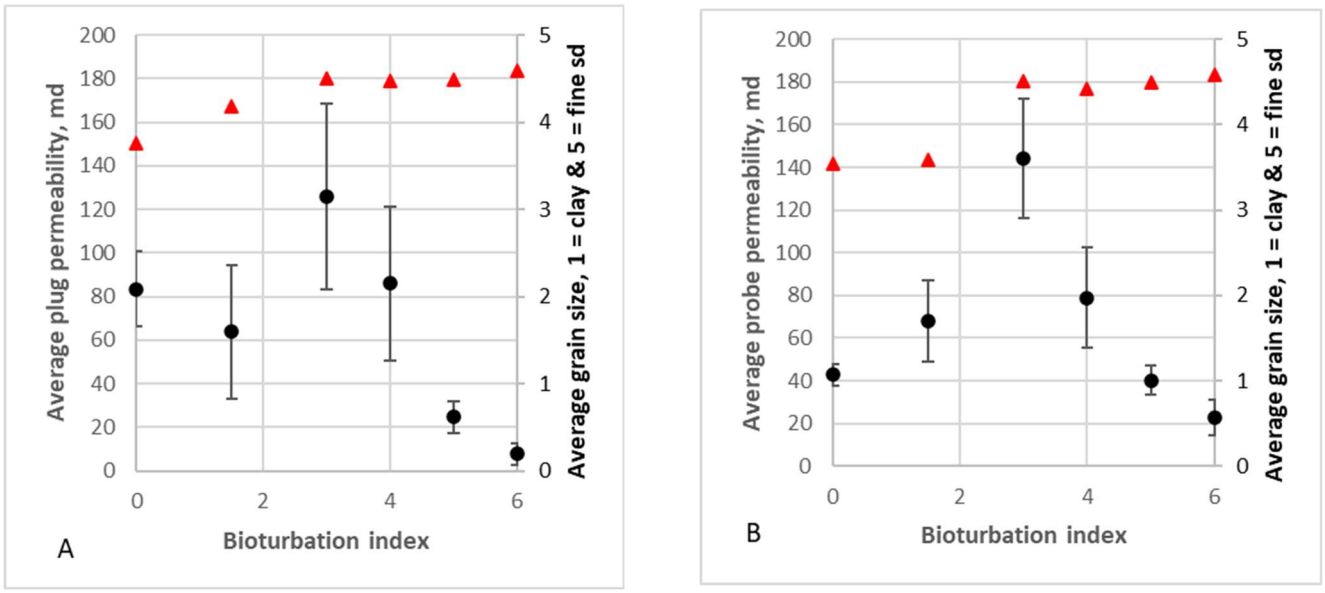

Figure 14. (**A**) Average plug and (**B**) probe permeabilities and their 68% probability standard errors (left axis) versus their bioturbation index values (x-axis). Average grain sizes for the same intervals appear in red triangles (right axis).

We find that, as Bi increases from Bi = 0 to Bi = 3, both average core-plug permeability and average probe permeability values increase, although the core-plug trend (Figure 14A) is not statistically significant, possibly reflecting plug sampling bias. As Bi increases above 3, the average permeability decreases until, at Bi = 6, the permeability falls below the Bi = 0 permeability. Using the 43 md average probe permeability at Bi = 0 as a reference, bioturbation with an index of 1 to 3 in tidally modified Strawn sediments with abundant mud drapes on sedimentary structures can increase the permeability by as much as 3.3 times, up to an intensity limit of Bi = 3. It appears that bioturbation can reduce the permeability by ½ at the intensity limit of Bi = 6. This variation is similar to what ref. [10] describe as a factor of 4 to 6 variation, but much less than refs. [33] 5 to 18 variation.

Notably, grain sizes also change over these intervals, so the average grain size was examined to determine if grain-size variations could explain the average permeability variations (Figure 14). The average grain sizes for sediments with Bi = 0 and Bi = 1.5 are nearly identical (Figure 5), hence grain size variations should not alone explain the increase in average permeability from 43 md to 68 md over this Bi change. Similarly, the average grain sizes for Bi = 3 through Bi = 6 are similar, suggesting that the probe permeability decrease from 144 md to 23 md is not simply related to grain size variability. However, the permeability increase from 68 md to 144 md across the Bi = 1.5 to Bi = 3 interval might be due, in part, to the grain size change from silt/very fine sand to very fine/fine sand. Permeability increases by factors of 3–5 have been observed when grain size changes from very fine to fine sand in both consolidated and unconsolidated media (e.g., refs. [34–36]). The variable relationship of permeability with the grain size and bioturbation index suggests multiple factors at work in modifying permeability, which have previously been poorly recognized at this resolution.

4. Discussion

One of the questions arising in mature field development is whether further analysis of core and wireline logs is warranted to reduce risk. This analysis can include re-evaluating wireline logs, re-examining previously plugged core, and, in our case, expending the time and cost of employing a tool such as the probe permeameter to refine permeability estimates. This study shows that the value added from probe permeameter measurements is considerable, and can help reduce development risks.

Several studies describe probe measurements in a geological context; some of these studies also had core-plug permeabilities available (e.g., refs. [19,23,24,36,37]). As we did have plug permeabilities but did not have the core plugs to make direct comparisons with probe values, we have described methods to compare the two and offer metrics for satisfactory performance. Furthermore, to our knowledge, this study uniquely integrates quantitative evaluations of bioturbation and grain size in the permeability analysis. Finally, this study shows the merits of probe permeability measurements for conventional petrophysical assessments such as net sand evaluation and permeability prediction from wireline density porosity measurements.

More precisely, the probe permeability measurements facilitated the following analyses.

1. Identifying the limitations of using core-plug porosity–permeability relationships to predict permeability using wireline porosity measurements. In this case, using the core-plug relationship will overpredict permeability by at least a factor of three in the three most permeable facies.
2. Illustrating the effects of core-plug sample volume on the permeability of heterolithic intervals. Core-plug permeabilities best represented the lower permeability mud-prone elements of these mixed-lithology sediments. Probe permeabilities were larger and reflected the less mud-bearing sediments.
3. Clarifying the effects of the full range of bioturbation intensity on permeability when similar analyses using core plugs gave statistically significant results only for the Bi = 5 and 6 levels.
4. Assessing permeable intervals missed by core-plug sampling. Probe values gave equal or larger net sand estimates than plug-based values.
5. Quantifying facies effects on permeability, particularly for facies KS1, KS2, and KS3 which, due to the fractured nature of the core, were poorly sampled by core plugs. In particular, KS3 is a moderately permeable facies, and its underrepresentation in core plugs can lead to underprediction of flow capacity.

These results suggest that including probe permeameter measurements will improve predictability and reduce risk in oil and gas exploration, as well as provide new insight into the finer-scale variability of rock properties. The probe permeameter reveals nuances in rock properties that are otherwise masked by low-resolution plug data and wireline logs that average out rock properties over greater thicknesses.

4.1. Resolving Facies and Bioturbation Effects on Permeability

Our analyses show that, in tidally modified deltaic deposits of the Strawn, moderate bioturbation can increase permeability up to a threshold, in our case Bi = 3, at which point permeability begins to decrease. These results may reflect lower- to moderate-intensity bioturbation increasing connectivity through heterolithic mud-rich intervals and mud drapes on sedimentary structures common in tidal systems (e.g., ref. [38]). Burrows similar to those found in the Strawn facies KS2 to KS5 (Figure 5) have been shown elsewhere to destroy finer-grained, mud-rich laminae on sandy sedimentary structures [10]. These burrows may increase isotropy and vertical permeability in reservoirs (e.g., Figure 5F) [10,33]. It has been shown that burrows generally tend to increase vertical permeability more than horizontal permeability [32]. Alternatively, higher bioturbation intensities can increase sediment mixing and clay distribution in pore spaces, and create poorly sorted stratigraphic intervals, reducing overall permeability [10]. Mud-filled burrows can also introduce mud into otherwise homogeneous, sandy facies (e.g., Figure 5E), further complicating the relationship.

Average grain size changes within intervals that exhibit bioturbation in the Strawn play a less important role than bioturbation level on permeability variation. The increases in grain size can, at most, partially explain the permeability increase as Bi changes from 1.5 to 3.

Facies control on permeability is important, particularly between the pair KM1 and KS1 and the remaining facies, KS2 through KS6. To a lesser extent, facies KS2, KS3, KS5,

and KS6 represent intermediate permeabilities while KS4 has the greatest permeability by at least a factor of two. All facies are very heterogeneous with all estimated C_V's greater than one. The most homogeneous facies with respect to permeability, KS2 and KS3 (C_V = 1.2 and 1.4, respectively), are the two facies with the least bioturbation. KS1 is also weakly bioturbated but has a large estimated C_V (= 1.7). However, with only four probe measurements and no core-plug measurements, this estimate has a large uncertainty towards smaller C_V values. Using a statistical procedure called the jackknife [20] p. 112, the actual C_V for KS1 is somewhere in the range 0.9 to 1.7 with 95% probability.

Facies KM1 introduces the effect of carbonate presence on permeability and heterogeneity. Of the seven facies, KM1 has the smallest median permeability and the highest C (= 1.9) (Table 5; Figure 9). KM1 is rarely bioturbated and poorly to moderately sorted, with a grain size ranging from silt to medium sand; it exhibits high angle planar to trough cross-stratification. In terms of grain size, bedforms, and degree of bioturbation, its characteristics are most closely aligned with KS4; however, the permeability analyses show it to be drastically different. The discrepancy is therefore mostly attributable to the presence of carbonate allochems and accompanying cement, which reduced permeability through occlusion of pores by calcite cement (Figure 5A,B).

4.2. Implications for Reservoir Performance

Our results have implications for two aspects of reservoir performance: productivity and trapping. Based on either the sample median or arithmetic average permeability values, and considering the type of facies found in the Strawn in the CB-Long C-16 core (tidally modified delta deposits), the most productive facies for oil and gas recovery in vertical wells of the Strawn are KS2 through KS6. These facies represent approximately 79% of the total sediments in the core, and 92% of the total flow capacity. KS1 has marginal productive capacity, while KM1 has almost no productive capacity. Productivity potential is therefore related to the combination of lithology, bioturbation, and cement. In comparisons of median probe values for six clastic facies and one mixed carbonate–clastic facies, carbonate-bearing facies were the least permeable by a factor of 10. This likely reflects permeability loss from carbonate cement in pore spaces (Figure 5A,B).

The productivity assessment is more complicated if (unfractured) horizontal wells are considered. This is because the productive advantage of horizontal wells over vertical wells is driven by the local permeability anisotropy, k_V/k_H, where the V and H subscripts refer to vertical and horizontal permeability, respectively. Reference [39] p. 100 recommends $k_V/k_H \geq 0.1$ for horizontal wells to be economically beneficial. No vertically orientated samples were taken in the CB-Long C-16 well to measure k_V; however, k_V can be estimated using the harmonic average of the probe permeabilities, whereas k_H can be estimated using the arithmetic average refs. [26,40].

Figure 15 shows the k_V/k_H ratios by averaging over one-, three-, and five-foot intervals using the probe data. The averages—harmonic or arithmetic—are separately applied over each of those three depth windows, and then the ratio is calculated. The choice of distance over which to calculate the averages appears to have little effect on the results. Intervals 2 and 3 have very few instances of $k_V/k_H < 0.1$; other intervals have one or more significant reduced k_V/k_H occurrences, which have different causes.

- Interval 1 (facies KS3, KS4, and KS5) contains medium- to fine-grained sandstone, low bioturbation intensity, but numerous thin mud-rich beds which reduce local vertical permeability.
- Interval 2 (facies KS5 and KS6) and Interval 3 (facies KS3 and KS5) have fine-grained sandstone and moderate to high bioturbation intensity. The bioturbation reduces permeability but makes the formation more isotropic.
- Interval 4 (facies KM1, KS3, and KS4) has variable grain size with low permeability carbonate intervals, significantly reducing k_V.
- Interval 5 (facies KM1, KS2, and KS3) has low-permeability siltstones alternating with thin fine-grained sandstones in the upper half and less heterogeneous higher

permeability fine-grained sandstones and carbonate in the lower half. The siliciclastic upper half has reduced k_V, likely reflecting the effect of siltstones, while the carbonate has both small k_H and k_V, giving near-unity k_V/k_H values.

- Interval 6 (facies KS5 and KS6) has low-permeability mudstone/siltstone at the top, a heavily bioturbated sandstone in the middle section, and low permeability siltstone at the bottom. These numerous lithological changes cause the k_V/k_H to decrease at the facies boundaries.

The highly variable nature of k_V/k_H indicates that the location of horizontal well placement will need careful consideration of potential facies trends in order to place the well in higher permeability and smaller k_V/k_H horizons. If the well is also fracture stimulated, then the small k_V/k_H occurrences may not be a significant control on productivity. Vertical fractures will penetrate thin muds and increase vertical permeability [41] p. 149. If hydrocarbon gas or CO_2 injection is implemented, k_V/k_H once again is a consideration because low permeability barriers may inhibit upward movement of gas. This can be an advantage by increasing contact and vertical sweep, or increasing trapping in the case of CO_2 sequestration. The lateral extent of the low-permeability carbonates in Interval 4 may be a major consideration on where injection should occur.

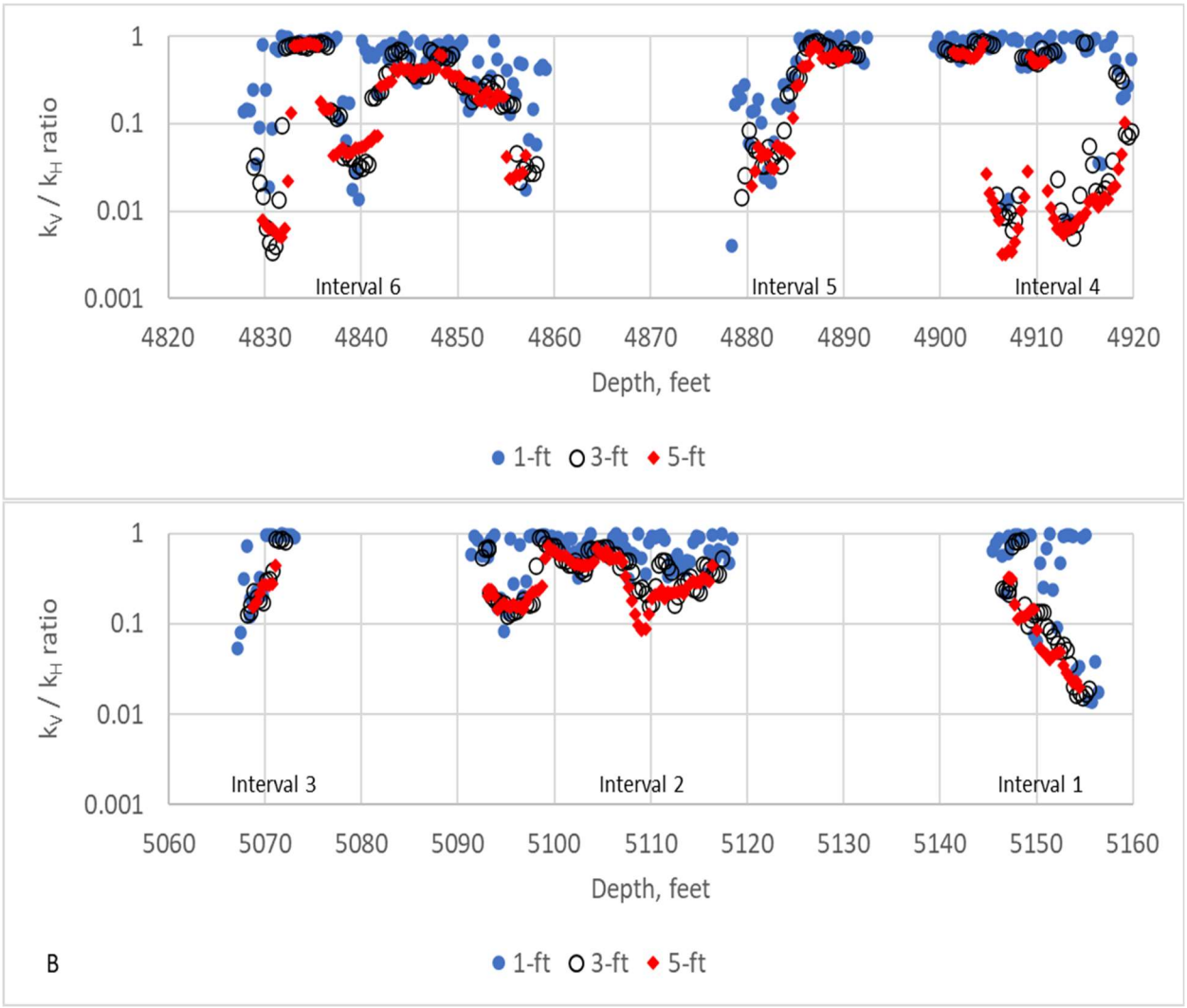

Figure 15. Probe-based permeability anisotropy for (**A**) the upper three intervals and (**B**) the lower three intervals. $k_V/k_H \leq 1$ because the arithmetic average always exceeds or equals the harmonic average [42] pp. 37–38.

Figure 15 and the Katz Field geology suggests a more complicated k_V/k_H behavior than [43] describe. Their Table 2 has $0.48 \leq k_V/k_H \leq 0.72$, with the First Sand having $k_V/k_H = 0.72$ and decreasing in the Second and Third Sands. Figure 15 indicates smaller k_V/k_H values apply and that there are important k_V/k_H reductions within sands. Interval 6, which includes all of the First Sand, has the probe-based $k_V/k_H = 0.075$, a factor of ten reduction compared to [43]'s value. Reference [44] found that decreasing k_V/k_H from 1 to 0.1 decreased CO_2 flood oil recovery by 15% in their modeling study. A similar oil production decrease was observed by ref. [45].

The above comparison requires further comment. Reference [43] states that the k_V/k_H values they list are for the reservoir and are based on core data, although they do not give the number and well locations. Figure 15 is for only one well, CB-Long C-16, but it has more intense sampling than core plugs. Given the east to northeast sourcing of these upper shoreface deposits, the central location of the CB-Long C-16 well suggests that k_V/k_H values could be larger to the northeast and smaller to the southwest.

4.3. Implications of Integrating Probe Permeameter Data

The probe permeameter measurements offered several benefits to the reservoir characterization process. Integrating probe data facilitated a more detailed characterization of porosity and permeability trends at high resolution for facies KS1, KS2, and KS3, comprising about 25% of the sampled core. Only four core plugs were taken in these facies. Probe permeability plotted against well-log density porosity revealed a different relationship than core-plug permeability versus core-plug porosity (Figure 13). This result has two significant implications. First, comparing density log-based permeability predictors against core-plug permeabilities may give misleading results because some facies may be underrepresented (poorly sampled) in the plug samples. Second, the application of the plug-scale porosity–permeability relationship in permeability prediction based on a density log can produce predictions which may be grossly in error, at least a factor of 3 in this case. Averaging was useful for some intervals to improve correlation of the probe and wireline data. Averaging, however, masked correlation in one highly heterogeneous interval, Interval 5 (Figure 12) because the coarser-grained intervals measured by the probe permeameter were too thin for the wireline density to resolve.

On a depth-by-depth basis, probe and plug permeability values are comparable. Probe permeabilities are generally equal to or smaller than plug permeability values when averaged over similar intervals. Some of this effect is the result of the more intensive sampling of finer-grained components of a facies using the probe permeameter. Net-to-gross sand ratio comparisons, however, show that probe measurements can also identify instances of higher permeability and net sand, which go undetected when using core-plug data. Of course, some thin expressions of permeable material, such as in Interval 5, may lack the lateral extent to contribute to economic production; however, if sufficiently thick and laterally extensive, these intervals could contribute a substantial volume to the reservoir.

Both the probe and plug permeabilities showed similar effects of variable bioturbation intensities on rock properties; however, statistically significant trends could only be identified using the probe permeameter measurements because we were able to obtain a higher-density, statistically representative dataset. The greater density of probe measurements also allowed estimates of k_V/k_H to be made. Core plugs sampled at lower-resolution one-foot spacing and with sample bias towards larger grain sizes and more consolidated intervals would not support this assessment. Ultimately, incorporating higher-resolution probe permeameter measurement into broader drill-core and wireline-log analyses can provide more statistically significant permeability datasets than core plugs and/or wireline logs alone can provide.

5. Conclusions

- As expected, sampling sufficiency was different for porosity and permeability. Core-plug porosities collected at one-foot spacing adequately sampled the formation, al-

though the sampling strategy is biased towards coarser-grained deposits. Core-plug permeability measurements, also collected from plugs at nominally one-foot spacing, were insufficient to characterize the permeability at ±20% tolerance but sufficient for some intervals at a ±50% tolerance. Facies KS1, KS2, and KS3 were particularly undersampled with respect to core plugs. Some of the undersampling was due to the mechanical limitations of the core-plugging procedure in friable intervals, especially for KS1. Limited sampling of KS2 and KS3, with permeabilities of 10 to 20 md, reduced the apparent productive potential of this part of the formation.

- Probe permeameter measurements correlated well with core-plug values on a point-by-point basis. Average permeameter measurements are equal to or are less than average plug permeabilities for any equivalent interval. This was mostly due to the inclusion of low-permeability probe measurements acquired from thin beds of muddy to shaley sediments that either could not be or were not sampled via core plugging.
- Repeat measurements were within a factor of two with 83% probability. Permeameter measurements allowed higher-resolution characterization of facies that were undersampled or unsampled by core plugs due to their disaggregated nature.
- Probe-based net sand proportions were equal to or exceeded plug-based values for four of the five intervals assessed, because higher-resolution probe permeameter measurements were able to identify additional thin lenses of high-permeability rock.
- Development of a permeability predictor based on well log porosities required probe permeameter measurements. Using the core-plug porosity–permeability relationship with the wireline density porosity overpredicted permeability by at least a factor of three for several facies (KS3, KS4, and KS5). A thickness-weighted average of the probe permeabilities correlated well with the wireline density log to give better predictions consistent with the well log resolution.
- The effect of bioturbation intensity on permeability is non-linear. As the bioturbation level increased from Bi = 0 to Bi = 3, average permeability increased. Grain-size variations can explain some but not all of this permeability change. As the bioturbation level increased from Bi = 3 to Bi = 6, average permeability decreased. These results may be related to a combination of lower-intensity bioturbation increasing connectivity through tidal mud drapes and higher bioturbation intensities increase sediment mixing and clay distribution in pore spaces, reducing overall permeability.
- The variabilities of permeability of all facies were very high, and core plugs were insufficient for the finer-grained intervals. Permeability measurements from the probe permeameter varied from 0.2 md to 45 md median values. Core-plug median permeabilities were within a factor of two for the facies with sufficient samples.

Probe-based permeabilities had coefficients of variation (C_V) in the 1.2 to 1.9 range, which represent very heterogeneous levels of permeability variation. Core-plug permeability variabilities were similar for facies that were sufficiently sampled. Two clastic facies, thin-bedded siltstones of KS1 and highly bioturbated fine to very fine sandstones of KS6, had permeability variabilities similar to the carbonate KM1 facies, which had the highest C_V of all tested facies.

Facies KS4 had the highest median permeability, with KS2, KS3, KS5, and KS6 representing somewhat lower permeabilities. KS4 exhibited a low degree of bioturbation and strongly defined bedding, which may improve permeability pathways; however, it was uncommon in the core, likely because it represents the most proximal deltaic channels in a core containing primarily distal deltaics and tidal shelf deposits. KS2, KS3, KS5, and KS6 are all more common, representing larger-scale portions of a deltaic complex; for these facies, a moderate degree of bioturbation appears to be the "sweet spot" where bioturbation improved flow pathways and thus permeability. A high degree of bioturbation appears to homogenize sediments, introduce mud into pore spaces, and reduce permeabilities. Facies KM1, although possessing similar grain size, bioturbation, and bedform characteristics to KS4, had significantly lower permeability due to the occlusion of pores by calcite cements.

Author Contributions: Conceptualization: J.L.J., P.P.F. and K.E.H. Data curation: J.L.J., P.P.F. and K.E.H. Formal analysis: J.L.J., P.P.F. and K.E.H. Investigation: J.L.J., P.P.F. and K.E.H. Methodology, J.L.J., P.P.F. and K.E.H. Project administration: P.P.F. Resources: P.P.F. Software: J.L.J. Supervision: P.P.F. Validation: J.L.J., P.P.F. and K.E.H. Visualization: J.L.J., P.P.F. and K.E.H. Writing–original draft: J.L.J. and P.P.F. Writing–review and editing: J.L.J., P.P.F. and K.E.H. All authors have read and agreed to the published version of the manuscript.

Funding: This investigation was supported by the Bureau of Economic Geology (BEG) State of Texas Advanced Resource Recovery (STARR) Program.

Data Availability Statement: The raw data supporting the conclusions of this article will be made available by the authors on request.

Acknowledgments: This research was supported by the Bureau of Economic Geology State of Texas Advanced Resource Recovery Program (STARR). We thank Eric Radjef for providing information on Strawn oil and gas production and Jasmeen Kaur for diligently collecting the probe permeameter measurements. We also thank Kinder Morgan Inc. for providing the CB-Long C-16 core and data. This document is approved by the Director of the Bureau of Economic Geology.

Conflicts of Interest: The authors declare no conflicts of interest.

References

1. Weber, K.J. How heterogeneity affects oil recovery. In *Reservoir Characterization*; Lake, L.W., Carroll, H.B., Jr., Eds.; Academic Press: Cambridge, MA, USA, 1986; pp. 487–544.
2. Lasseter, T.J.; Waggoner, J.R.; Lake, L.W. Reservoir heterogeneities and their influence on ultimate recovery. In *Reservoir Characterization*; Lake, L.W., Carroll, H.B., Jr., Eds.; Academic Press: Cambridge, MA, USA, 1986; pp. 545–559.
3. Ellis, D. The Rough Gas Field: Distribution of Permian aeolian and non-aeolian reservoir facies and their impact on field development. In *Characterization of Fluvial and Aeolian Reservoirs*; North, C.P., Prosser, D.J., Eds.; Geological Society Spec. Pub.: London, UK, 1993; Volume 73, pp. 265–278.
4. Dykstra, H.; Parsons, R.L. The prediction of oil recovery by waterflood. In *Secondary Recovery in the USA*, 2nd ed.; American Petroleum Institute: New York, NY, USA, 1950; pp. 160–174.
5. Hurst, A.; Goggin, D.J. Probe permeametry: An overview and bibliography. *AAPG Bull.* **1995**, *79*, 463–473.
6. Wright, W.R. Pennsylvanian (upper Carboniferous) paleodepositional evolution of the greater Permian Basin, Texas and New Mexico: Depositional systems and hydrocarbon reservoir analysis. In *Anatomy of a Paleozoic Basin: The Permian Basin, USA*; Ruppel, S.C., Ed.; Bureau of Economic Geology Report of Investigation 285; AAPG Memoir 118; The University of Texas at Austin: Austin, TX, USA, 2020; Volume 2, Chapter 18; pp. 159–184.
7. Pranter, M.J.; Grayson, R.C., Jr. "Lower Strawn" submarine fan complex and associated depositional systems. In *Transactions of the 1990 AAPG Southwest Section Convention*; Gibbs, C.M., Reynolds, C.W., Tucker, W., Ritchie, J., Eds.; American Association of Petroleum Geologists: Tulsa, OK, USA, 1990; pp. 103–120.
8. Roberts, A.K.; Ambrose, W.A.; Flaig, P.P.; Steel, R.J.; Olariu, C. *Controls on Facies Variability and Distribution During the Pennsylvanian Glacial Period from the Lower Strawn Group*; The American Association of Petroleum Geologists Bulletin: Fort Worth Basin, TX, USA, 2022; Volume 106, pp. 1679–1702. [CrossRef]
9. S&P Global Commodity Insights. [Includes Data Current as of June 2024]: 15 Inverness Way East, Englewood, CO, USA, 2024; 80112. Available online: https://www.spglobal.com/commodity-insights/en?utm_campaign=q4_2024_global-inbound-website-ad-branded_products-services-brand&utm_medium=cpc&utm_source=google&gclid=EAIaIQobChMIkuC5qb6cigMVOhStBh0RXjACEAAYASAAEgKOvfD_BwE (accessed on 21 November 2024).
10. Tonkin, N.S.; McIlroy, D.; Meyer, R.; Moore-Turpin, A. Bioturbation influence on reservoir quality: A case study from the Cretaceous Ben Nevis Formation, Jeanne d'Arc Basin, offshore Newfoundland, Canada. *AAPG Bull.* **2010**, *94*, 1059–1078. [CrossRef]
11. Mukhtar, M.H.; Hatzignatiou, D.G.; Ehlig-Economides, C. Extended aquifer system pressure behavior under carbon storage. *SPE J.* **2024**, *29*, 5101–5119. [CrossRef]
12. Mullins, J.; Pierce, C.; Rieke, H.; Howell, J. Aeolian sand dune sedimentary architecture is key in determining the "slow gas effect" during gas field production performance. *SPE J.* **2022**, *27*, 1354–1366. [CrossRef]
13. Mellal, I.; Malki, M.L.; Latrach, A.; Ameur-Zaimech, O.; Bakelli, O. Multiscale formation evaluation and rock types identification in the Middle Bakken Formation. In Proceedings of the SPWLA 64th Annual Logging Symposium, Lake Conroe, TX, USA, 10–14 June 2023. Paper SPWLA-2023-0012.
14. La Croix, A.D.; Gingras, M.K.; Dashtgard, S.E.; Pemberton, S.G. Computer modeling bioturbation: The creation of porous and permeable fluid-flow pathways. *AAPGBull.* **2012**, *96*, 545–556. [CrossRef]

15. Brown, A.; Ambrose, W.A.; Carr, D.L. Supplement to Guidebook 14: The University of Texas at Austin. In *Bureau of Economic Geology Field Trip Guidebook*; Bureau of Economic Geology, University of Texas: Austin, TX, USA, 2009; 104p.
16. Flaig, P.P.; Hattori, K.E.; Hasiotis, S.T.; Boucher, L.; Buntin, C.; Roberts, A.; Lorente, M.A.; Moscardelli, L. *Complex Clastics and Associated Carbonates of the Strawn Formation: Re-Evaluation of Deposystem Interpretations From Core and Outcrop-Based Investigations*; American Association of Petroleum Geologists Southwest Section Meeting: Wichita Falls, TX, USA, 2023.
17. Taylor, A.M.; Goldring, R. Description and analysis of bioturbation and ichnofabric. *J. Geol. Soc.* **1993**, *150*, 141–148. [CrossRef]
18. Jensen, J.L.; Uroza, C.A. Testing and application of a probe permeameter in the lower Wilcox formation, onshore Texas, USA. *Petrophysics* **2024**, *65*, 665–681. [CrossRef]
19. Hurst, A.; Rosvoll, K.J. Permeability variations in sandstones and their relationship to sedimentary structures. In *Reservoir Characterization II*; Lake, L.W., Carroll, H.B., Wesson, T.C., Eds.; Academic Press: Cambridge, MA, USA, 1991; pp. 166–196.
20. Jensen, J.L.; Lake, L.W.; Corbett, P.W.M.; Goggin, D.J. *Statistics for Petroleum Engineers and Geoscientists*, 2nd ed.; Elsevier: Amsterdam, The Netherlands, 2000; 338p.
21. Corbett, P.W.M.; Jensen, J.L. Lithological and zonal porosity-permeability distributions in the Arab-D Reservoir, Utmaniyah Field, Saudi Arabia: Discussion. *AAPG Bull.* **2000**, *84*, 1365–1367.
22. Lake, L.W. *Enhanced Oil Recovery*; Prentice Hall: Englewood Cliffs, NJ, USA, 1989; 550p.
23. Meyer, R.; Krause, F.F. A comparison of plug-derived and probe-derived permeability in cross-bedded sandstones of the Virgelle Member, Alberta, Canada: The influence of flow directions in probe permeametry. *AAPG Bull.* **2001**, *85*, 477–489.
24. Corbett, P.W.M.; Jensen, J.L. Variation of reservoir statistics according to sample spacing and measurement type for some intervals in the Lower Brent Group. *Log Anal.* **1992**, *33*, 22–41.
25. Nordahl, K.; Ringrose, P.S. Identifying the representative elementary volume for permeability in heterolithic deposits using numerical rock models. *Math. Geosci.* **2008**, *40*, 753–771. [CrossRef]
26. Morton, K.; Thomas, S.D.; Corbett, P.W.M.; Davies, D. Detailed analysis of probe permeameter and interval pressure transient test permeability measurements in a heterogeneous reservoir. *Pet. Geosci.* **2002**, *8*, 209–216. [CrossRef]
27. Okwoli, E.; Potter, D.K. Probe screening techniques for rapid, high-resolution core analysis and their potential usefulness for energy transition applications. *Petrophysics* **2023**, *64*, 640–655. [CrossRef]
28. Cobb, W.M.; Marek, F.J. Net pay determination for primary and waterflood depletion mechanisms. In Proceedings of the SPE Annual Technical Conference and Exhibition, New Orleans, LA, USA, 27–30 September 1988. Paper SPE 48952.
29. Hoaglin, D.C.; Mosteller, F.; Tukey, J.W. *Understanding Robust and Exploratory Data Analysis*; John Wiley and Sons: New York, NY, USA, 1983; 447p.
30. Wendt, W.A.; Sakurai, S.; Nelson, P.H. Permeability prediction from well logs using multiple regression. In *Reservoir Characterization*; Lake, L.W., Carroll, H.B., Jr., Eds.; Academic Press: Cambridge, MA, USA, 1986; pp. 181–221.
31. El-Shokir, E.M.; Alsughayer, A.A.; Al-Ateeq, A. Permeability estimation from well log responses. *J. Can. Pet. Technol.* **2006**, *45*, 41–46.
32. Gingras, M.K.; Baniak, G.; Gordon, J.; Hovikoski, J.; Konhauser, K.O.; La Croix, A.; Lemiski, R.; Mendoza, C.; Penberton, S.G.; Polo, C.; et al. Porosity and permeability in bioturbated sediments. *Dev. Sedimentol.* **2012**, *64*, 837–868. [CrossRef]
33. Singh, A.; Pharate, N.; Desai, B.G. Assessing the impact of bioturbation on reservoir quality: Integrated spontaneous imbibition, pressure decay profile permeability and pore-throat characterization study of the Cretaceous Bhuj formation, Kachchh basin, India. *Geoenergy Sci. Eng.* **2023**, *228*, 212000. [CrossRef]
34. Beard, D.C.; Weyl, P.K. Influence of texture on porosity and permeability of unconsolidated sand. *AAPG Bull.* **1973**, *57*, 349–369.
35. Pettijohn, F.J.; Potter, P.E.; Siever, R. *Sand and Sandstone*, 2nd ed.; Springer: New York, NY, USA, 1987; 553p.
36. Willis, B.J. Permeability structure of a compound valley fill in the Cretaceous Fall River Formation of South Dakota. *AAPG Bull.* **1998**, *82*, 206–227.
37. Solano, N.A.; Soroush, M.; Clarkson, C.R.; Krause, F.F.; Jensen, J.L. Modeling core-scale permeability anisotropy in highly bioturbated "tight oil" reservoir rocks. *Comput. Geosci.* **2017**, *21*, 567–593. [CrossRef]
38. Flaig, P.P.; Hasiotis, S.T.; Prather, T.J.; Burton, D. Characteristics of a Campanian delta deposit controlled by alternating river-floods and tides: The Loyd Sandstone, Rangely Anticline, Colorado, U.S.A. *J. Sediment. Res.* **2019**, *89*, 1181–1206. [CrossRef]
39. Baker, R.O.; Yarranton, H.W.; Jensen, J.L. *Practical Reservoir Engineering and Characterization*; Gulf Professional Publishing: Waltham, MA, USA, 2015; 521p.
40. Thomas, S.D.; Corbett, P.W.M.; Jensen, J.L. Upscaling vertical permeability within a fluvio-aeolian reservoir. In Proceedings of the Fourth International Reservoir Characterization Technical Conference Proceedings, Houston, TX, USA, 2–4 March 1997; pp. 583–597.
41. Joshi, S.D. *Horizontal Well Technology*; PennWell Books: Tulsa, OK, USA, 1991; 535p.
42. Kendall, M.; Stuart, A. *The Advanced Theory of Statistics*; Charles Griffin and Co.: London, UK, 1977; Volume 1, 472p.
43. Smith, D.J.; Kelly, T.R.; Schmidt, D.L.; Bowden, C.E. Katz (Strawn) Unit miscible CO_2 project: Design, implementation, and early performance. In Proceedings of the Eighteenth SPE Improved Oil Recovery Symposium, Tulsa, OK, USA, 14–18 April 2012; Paper SPE 154023.

44. Ren, B.; Jensen, J.L.; Lake, L.W.; Duncan, I.D.; Male, F. Analysis of vertical permeability and its influence on CO_2 enhanced oil recovery and storage in a carbonate reservoir. *SPE Reserv. Eval. Eng.* **2022**, *25*, 414–432. [CrossRef]
45. Campero, M.F.; Nwonodi, C.; Onwuchekwa, C.; Eka, K.; Adenalye, O.; Igogo, A.; Adekoya, O.; Ebere, A. Kv/Kh in heterogeneous reservoirs of a brown field in the Niger Delta of Nigeria–valuable uncertain parameter for assisted history matching. In Proceedings of the SPE Nigeria Annual International Conference and Exhibition, Lagos, Nigeria, 6–7 August 2014; Paper SPE 172450.

Disclaimer/Publisher's Note: The statements, opinions and data contained in all publications are solely those of the individual author(s) and contributor(s) and not of MDPI and/or the editor(s). MDPI and/or the editor(s) disclaim responsibility for any injury to people or property resulting from any ideas, methods, instructions or products referred to in the content.